iScience

CellPress
OPEN ACCESS

Article

VDAC1-interacting molecules promote cell death in cancer organoids through mitochondrial-dependent metabolic interference

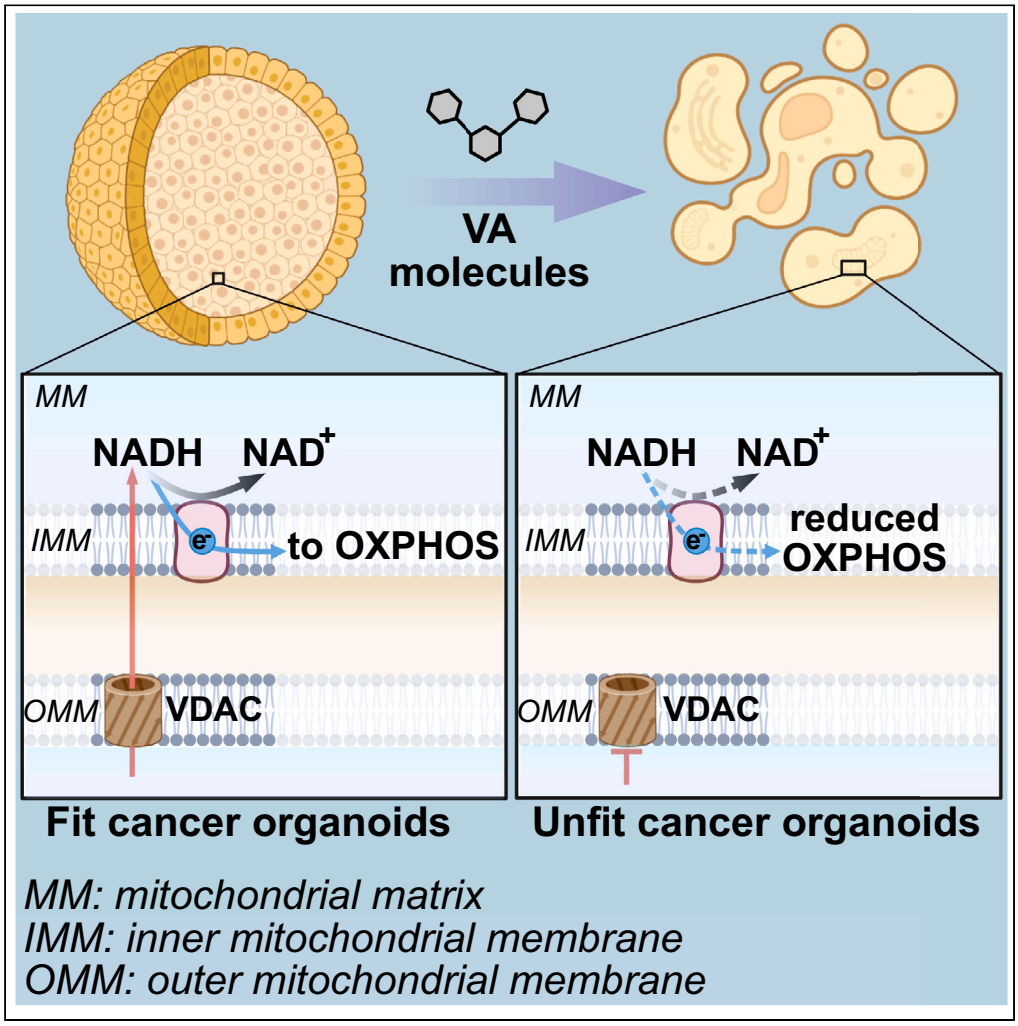

Stefano Conti Nibali, Silvia De Siervi, Enrico Luchinat, ..., Cristian Turato, Cristina Arrigoni, Marco Lolicato

cristina.arrigoni01@unipv.it (C.A.)
marco.lolicato@unipv.it (M.L.)

Highlights

Mitochondrial metabolism can be targeted for cancer treatment via VDAC1 porin

New VA (VDAC Antagonists) molecules bind VDAC1 *in vitro* with micromolar affinity

VA molecules compete with NADH causing mitochondrial distress in cancer cells

VA molecules reduce cell viability of cholangiocarcinoma organoids

Conti Nibali et al., iScience 27, 109853
June 21, 2024
https://doi.org/10.1016/j.isci.2024.109853

iScience

CellPress
OPEN ACCESS

Article

VDAC1-interacting molecules promote cell death in cancer organoids through mitochondrial-dependent metabolic interference

Stefano Conti Nibali,[1,8,9] Silvia De Siervi,[1,8] Enrico Luchinat,[2,3] Andrea Magrì,[4] Angela Messina,[4] Lorenza Brocca,[1] Stefania Mantovani,[5] Barbara Oliviero,[5] Mario U. Mondelli,[5,6] Vito De Pinto,[7] Cristian Turato,[1] Cristina Arrigoni,[1,*] and Marco Lolicato[1,10,*]

SUMMARY

The voltage-dependent anion-selective channel isoform 1 (VDAC1) is a pivotal component in cellular metabolism and apoptosis with a prominent role in many cancer types, offering a unique therapeutic intervention point. Through an *in-silico*-to-*in-vitro* approach we identified a set of VA molecules (VDAC Antagonists) that selectively bind to VDAC1 and display specificity toward cancer cells. Biochemical characterization showed that VA molecules can directly interact with VDAC1 with micromolar affinity by competing with the endogenous ligand NADH for a partially shared binding site. NADH displacement results in mitochondrial distress and reduced cell proliferation, especially when compared to non-cancerous cells. Experiments performed on organoids derived from intrahepatic cholangiocarcinoma patients demonstrated a dose-dependent reduction in cell viability upon treatment with VA molecules with lower impact on healthy cells than conventional treatments like gemcitabine. VA molecules are chemical entities representing promising candidates for further optimization and development as cancer therapy strategies through precise metabolic interventions.

INTRODUCTION

Cancer, a complex and devastating disease, continues to challenge medical researchers worldwide. Successful development of cancer therapy has roots in understanding derailed physiological mechanisms observed in cancer cells, including metabolic rewiring, used by tumor cells to escape immunosurveillance thus leading to apoptosis evasion and uncontrolled proliferation.[1]

The Warburg effect, a metabolic alteration observed in many cancer cell types, has garnered significant attention as a possible cancer cell-selective target mechanism. In this metabolic alteration, glucose metabolism is predominantly directed toward biosynthetic pathways required for rapid cell proliferation and growth. In this context, both glycolysis and oxidative phosphorylation (OXPHOS) are simultaneously enhanced to thrive cancer cell proliferation[2] by tampering with mitochondrial metabolism.

The maintenance of mitochondrial metabolism relies on the balanced flow of respiratory substrates, nucleotides (ATP, ADP), and ions into and out of mitochondria. Voltage-dependent anion-selective channels (VDAC) in the outer mitochondrial membrane (OMM) play a crucial role in maintaining cell bioenergetic, transporting most anionic metabolites and small ions in and out the mitochondria. In mammals, three different isoforms (VDAC1, VDAC2, and VDAC3) as 28–32 kDa proteins with around 70% sequence similarity.[3] Among the isoforms, VDAC1 is in charge of the regulation of mitochondria-mediated apoptosis by partnering with anti- and pro-apoptotic proteins.[4] Under physiological conditions, VDAC1 interacts with anti-apoptotic Bcl-2 family members to inhibit apoptosis, while in the presence of cellular stress or apoptotic stimuli the channel drives the activation of the intrinsic apoptotic pathway and eventually leads to programmed cell death.[5]

There is mounting evidence that VDAC1 interacts with the N-terminal portion of the glycolytic enzymes hexokinases (HKs).[6,7] The interaction between HKs and VDAC1 has a dual effect: (1) it prevents the interaction of the porin with pro-apoptotic factors[8] and (2) it provides tumor cells with a metabolic advantage through the "Warburg effect". Colocalization of HK proteins and VDAC1 gives HKs preferential access to the

[1]Department of Molecular Medicine, University of Pavia, Pavia, Italy
[2]Department of Chemistry "Ugo Schiff", University of Florence, via della Lastruccia 3, 50019 Firenze, Italy
[3]Consorzio Interuniversitario Risonanze Magnetiche di Metallo Proteine – CIRMMP, Via Luigi Sacconi 6, 50019 Sesto Fiorentino, Italy
[4]Department of Biological, Geological and Environmental Sciences, University of Catania, Catania, Italy
[5]Research Department, Division of Clinical Immunology—Infectious Diseases, Fondazione IRCCS Policlinico San Matteo, Pavia, Italy
[6]Department of Internal Medicine and Therapeutics, University of Pavia, Pavia, Italy
[7]Department of Biomedical and Biotechnological Sciences, Section of Biology & Genetics, University of Catania, Catania, Italy
[8]These authors contributed equally
[9]Present address: Department of Biomedical and Biotechnological Sciences, Section of Biology & Genetics, University of Catania, Catania, Italy
[10]Lead contact
*Correspondence: cristina.arrigoni01@unipv.it (C.A.), marco.lolicato@unipv.it (M.L.)
https://doi.org/10.1016/j.isci.2024.109853

ATP produced within mitochondria. Interestingly, high expression of both VDAC1 and HKs has been observed in many cancer types.[6,7,9–13] This allows cancer cells to maintain a high rate of glycolysis, even under aerobic conditions, which provides a continuous supply of building blocks for rapid cell proliferation.[14] Overall, the altered VDAC1 expression and function appear related to highly metabolically active and energy-demanding cancer cells, suggesting that the channel may act as an oncogene prompting the tumor progression by different molecular mechanisms, including the deregulation of apoptosis.[15–17] Thus, the specific role of VDAC1 in this pathological context, together with its druggability strengthened the suitability of these proteins as pharmacological targets.[18,19] To this date several molecules and peptides have been developed to modulate VDAC1 activity to impair energy homeostasis, proliferation, and apoptosis in cancer cells. To date, three distinct classes of molecules or peptides have been tested aimed to (i) interfere with the VDAC1-HKs interaction; (ii) modulate the electrophysiological activity of the channel; (iii) affect the expression levels of VDAC1 gene.[20–28] However, in most cases, the identified molecules have not met the need of a cancer cell-specific action and/or their binding pocket has not been fully characterized.

In light of this, through an initial *in silico* approach and subsequent thorough biochemical binding assays and NMR spectroscopy, we have identified a set of chemical entities, hereafter identified *VA,* i.e., VDAC-Antagonist. These molecules are characterized by a three-ring architecture and they specifically bind VDAC1 in a defined pocket that partially superposes that one of NADH.[29] Binding competition assays revealed that VA molecules compete with NADH in a dose-response manner, resulting in the interference of its binding to the channel.

NADH is a known VDAC1 modulator[30] and our experiments showed that the displacement of NADH from VDAC1 resulted in lower mitochondrial oxygen consumption, suggesting mitochondrial distress.

When tested in cell cultures, VA molecules reduced cell proliferation and promoted cell death in living organoid settings in a dose-response manner.

Altogether these findings suggest that cancer cell proliferation can be effectively halted by VA molecules treatment, leaving the surrounding healthy cells unaffected. This result strengthens the observations about the important role of VDAC as governor of cell fate.

RESULTS

High-throughput screening identifies five VDAC1 binders

The overexpression of VDAC1 in highly glycolytic cancer cells prompted us to develop a workflow for the identification of chemical entities able to decrease energy production in cancer cells. VDAC1 is a β-barrel channel constituted by 19 anti-parallel β-strands and an N-terminal α-helix (Figure 1A). The N-terminal helix is a highly mobile element fundamental for the channel gating[31] and for the interaction of VDAC1 with the cytosolic protein partners.[32] To date, the N-terminal helix has been structurally observed inside the β-barrel where it separates the channel lumen from a small cavity toward the barrel. Part of this groove accommodates the nicotinamide moiety of NADH (Figure 1B), the main oxidizing power accumulator from the Tricarboxylic acid (TCA) cycle inside the mitochondria.

The rationale behind the drug discovery was to hamper the interaction of VDAC1 N-terminal helix with anti-apoptotic factors by stabilizing its interaction within the barrel cavity. Thus, we partnered with Atomwise Inc. (San Francisco, CA) for the *in silico* search of molecules able to staple VDAC1 N-terminal helix within the cavity of the β-barrel. We identified a putative large binding area composed of the N-terminal helix (residues 1–21) and β-strands 12–18 (Figures 1A and 1C). This region includes the NADH anchoring point (Figures 1B and 1C).[29]

Atomwise technology screened a proprietary chemical library of millions of compounds and identified 70 hits that were experimentally tested for *in vitro* binding with a suite of assays.

First, in order to maximize the throughput, we tested the seventy molecules by measuring the VDAC1 protein thermal denaturation in absence and in presence of the compounds, relying on the correlation between an increase of the apparent denaturation temperature of the purified VDAC1 protein and a stabilization effect given by the bound molecule. Out of the seventy molecules, five compounds (hereafter called VA, VDAC-Antagonist) stabilized the apparent VDAC1 unfolding temperature by > 3°C (Figures 1E–1I), a significant change consistent with protein-molecule binding.[33]

The five selected molecules were graduated to a biophysical characterization to confirm *in vitro* binding to the purified VDAC1.

The chemical identity of the five molecules was confirmed by ^{1}H-NMR (Figure S1). ^{19}F NMR was additionally recorded for the molecules VA-D10, VA-C4, and VA-C1 which present three (VA-C1) and one (VA-D10 and VA-C4) fluorine atom, respectively.

The ^{19}F nucleus is highly sensitive to changes in the chemical environment and is absent in biological macromolecules and detergents, making it an ideal probe for monitoring protein-ligand interactions in complex mixtures.[34,35] Therefore, the presence of fluorine atoms was exploited to test the direct binding to VDAC1 by monitoring the ^{19}F signal of each compound in a micelle-containing buffer in the absence and in the presence of VDAC1. All three compounds experienced line broadening even without VDAC1, likely due to non-specific interaction with the micelles. The presence of VDAC1 caused further line broadening (VA-C1 and VA-D10) and/or shifting (VA-C4 and VA-D10) of the ^{19}F resonance in the spectrum of each molecule (Figure 2), thereby indicating direct binding to the protein.

These experiments confirmed that out of seventy molecules obtained from the *in silico* screening five are *in vitro* binders, so we focused on this set for biophysical characterization of the binding mode and affinity.

VA molecules share part of the binding site with NADH and bind VDAC1 with micromolar affinity

We docked the VA molecules into the target binding region identified in the *in silico* screening. All five molecules share a "*V shape*" conformation and three aromatic rings in their structure (Figures 1D–1J). For simplicity we call the three rings L- (left), C- (central) and R- (right). All five molecules present the three-ringed structure, except for VA-C1 which has a pseudo-C-ring conformation.

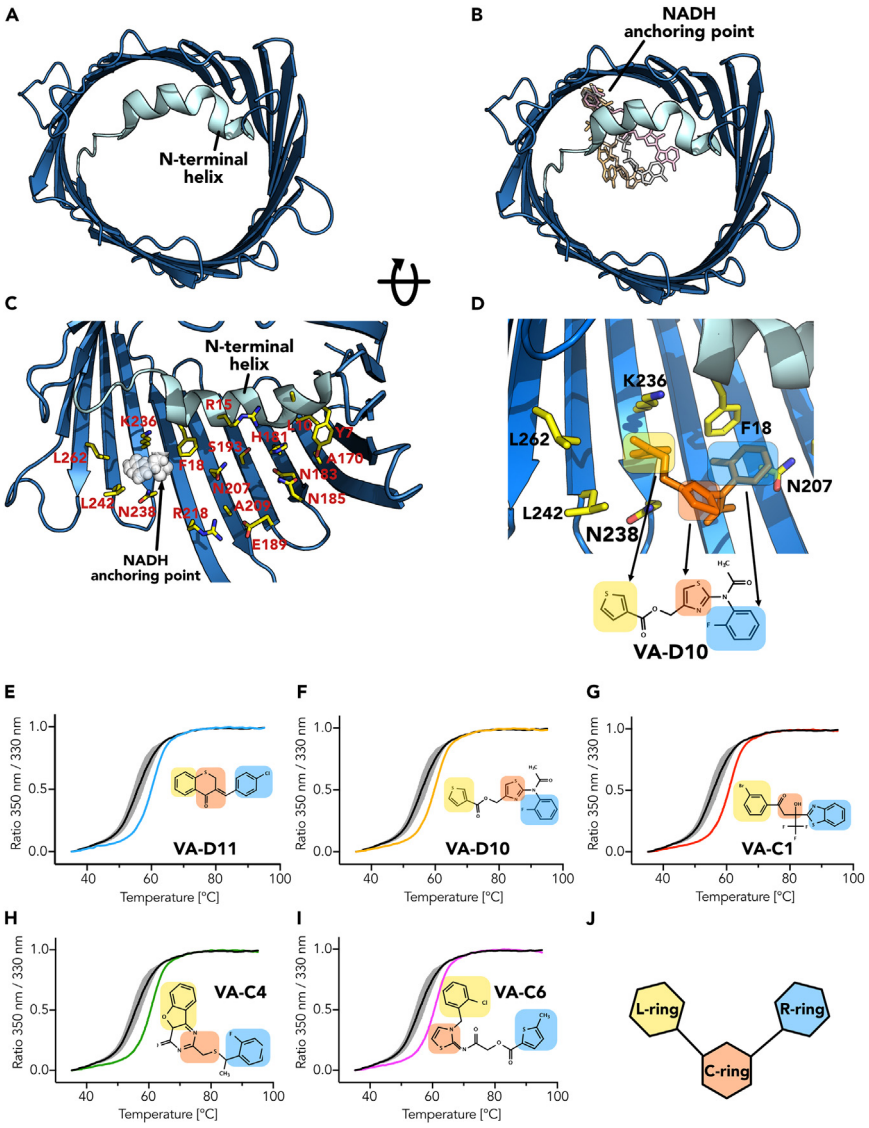

Figure 1. VDAC1 architecture and small molecule identification

(A) Cartoon representation of mouse VDAC1 crystal structure (PDB: 3EMN). In blue is identified the β-strand topology of the channel, and in cyan, its N-terminal α-helix.

(B) Selected poses of NADH bound to the channel (PDB: 6TIR), with its nicotinamide anchoring point highlighted.

(C) The large groove between VDAC1 N-terminal helix and the β-barrel used as a target for the AtomNet drug discovery campaign. NADH anchoring point is indicated.

(D) Close-up view of the putative VA compounds binding pocket, showing the VA-D10 molecule docked in the pocket and assuming a V-shaped conformation.

(E–I) Representative denaturation curves of mVDAC1 (0.9 mg/mL) in LDAO after treatment with different VA molecules at a final concentration of 1 mM. Black curves represent the denaturation profile of the protein pre-treated with DMF (0.5%), and the colored ones the protein pre-treated with the indicated VA molecules. Temperature denaturation inflection point (T_i) shifts toward higher temperatures in the presence of VA molecules VA-D11 (+4.7 ± 0.1); VA-D10 (+4.9 ± 0.1); VA-C1 (+4.6 ± 0.1); VA-C4 (+3.6 ± 0.2); VA-C6 (+4.6 ± 0.1), indicating protein stabilization/binding. Data are expressed as mean ± SEM (n = 3).

(J) Three-rings architecture and overall shape shared by all VA molecules.

From docking we obtained several poses revealing that all the molecules shared part of the NADH binding pocket (Figure 1D). In particular, VA molecules are framed by residues F18 (π−π interaction with R-ring), N207, R218 (cation- π interaction with C-ring), K236 (cation- π interaction with L-ring) and N238. Considering the dynamics of the NMR structure, the NADH nicotinamide moiety seems to overlap with only the L-ring of the docked VA molecules and only marginally involves the N-terminal helix, which makes more contacts with the more flexible part of NADH.[29] In contrast, the three-ringed architecture of the VA molecules enables a firm anchoring of the N-terminal helix to the barrel by the insertion of the helix F18 into the V shaped compound (Figure 1D).

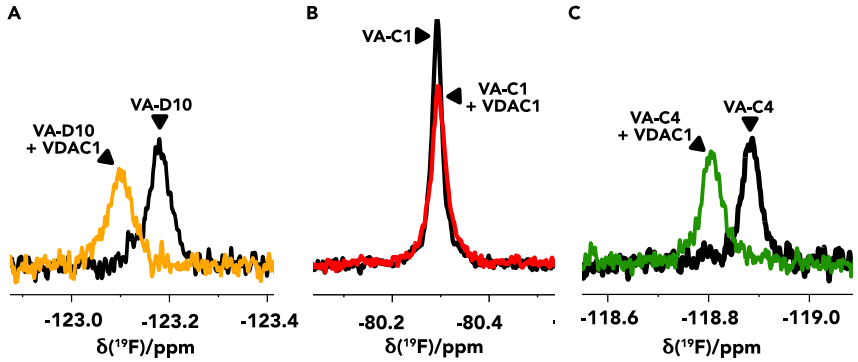

Figure 2. VA molecule binding measured by ^{19}F NMR

(A–C) ^{19}F NMR spectra of indicated VA molecules in LDAO buffer (black lines) and in the presence of 5μM mVDAC1 (colored lines). VA-D10 (A) and VA-C4 (C) significantly move their chemical shifts upon VDAC1 binding. VA-C1 (B) shows a reduction and broadening of its peak upon VDAC1 interaction. (See also Figure S1).

To test the hypothesis that VA molecules and NADH share the binding pocket, we carry out a fluorescence polarization (FP) assay based on the intrinsic fluorescence of NADH molecules (λ_{ex} = 355, λ_{em} = 460 nm). We measured the change in FP upon binding of NADH to purified VDAC1 and we fitted the data with a Hill curve obtaining the apparent affinity (K_D = 6.80 ± 0.06, Figure 3A). We then used a concentration of NADH of 5μM to perform a competition assay in the presence of increasing VA molecules concentrations (Figures 3B–3F). All five molecules showed a decrease in the FP signal in a dose-response manner, confirming the competition with NADH binding with an apparent K_D in the micromolar range (K_DVA-D11 = 15.9 ± 0.7, K_DVA-D10 = 18.5 ± 0.2, K_DVA-C1 = 18.7 ± 0.3, K_DVA-C4 = 19.4 ± 0.4, K_DVA-C6 = 18.7 ± 0.6).

Based on the key residues identified in the docking simulations we designed mutations in VDAC1 to confirm the binding and test the importance of the putative interactions.

We tested mutations that supposedly either stabilize or destabilize the binding of VA molecules by means of thermal denaturation assays (Figures 4A–4F) on purified VDAC1. If the molecules bind in the V-shape conformation, introducing positive charges or aromatic residues in place of neutral amino acids (N207R, N238 K/F) should strengthen the interactions with the aromatic rings. On the opposite, removing the key π−π interaction with R-ring (F18A) and the cation-π interaction with L-ring (K236A), should lower the affinity of the molecule. To quantify the effect of the mutations on the binding we calculated the difference of the inflection temperature (ΔΔTi) of each mutant in absence or presence of the molecules ($\Delta Ti_{mut(VA\_mol)}$-$\Delta Ti_{mut(DMSO)}$) compared to those measured for VDAC1 wild-type ($\Delta Ti_{wt(VA\_mol)}$-$\Delta Ti_{wt(DMSO)}$). A positive value was observed for mutants N238K, N238R, N207R, N238F, R218Y consistent with a higher thermostability of these VDAC1 mutants when bound to the molecules (Figure 4). On an opposite trend, alanine substitutions of charged and aromatic residues (K236A, F18A) resulted in a negative difference of the relative unfolding temperatures for all the five molecules. The significance of the differences measured was also confirmed by the unchanged Ti of the mutant in control conditions compared to the wild-type (Table S1), suggesting that these mutations *per se* do not alter the overall stability of the protein.

The thermal denaturation assays confirmed the docking-generated hypothesis of the binding mode of the VA molecules showing a decreased apparent affinity for the destabilizing mutations and an improved binding for the stabilizing mutations (Table 1).

To quantify mutations effect more rigorously, we performed FP assays of the two VDAC1 mutants, K236A and N238K (Figure 5).

VDAC1 K236A and N238K, indeed, show respectively decreased and increased affinity for the molecules compared to the wild-type channel (Table 2). Notably, the NADH affinity for the mutants did not change (Figure S2), suggesting that residues K236 and N238, previously identified as part of the NADH binding site,[29] do not contribute significantly in NADH binding. This can be explained by the high mobility of the NADH molecule resolved inside the pore in the NMR structure where the only well-defined region of the NADH binding pocket consists in the nicotinamide moiety.[29] The NMR consensus models show that this part of the molecule binds to several residues within VDAC1 β-barrel and N-terminal helix, however, N238 makes polar contacts with NADH only in 50% of the poses and only in one of them the H-bond involves the side chain of the asparagine. K236, instead, is part of the binding pocket but its side chain is too far to interact with the nicotinamide moiety.

Compared to NADH, VA molecules have less steric hindrance and are heavily affected by the mutations, suggesting that the predicted binding pocket is localized within the framing residues that we characterized.

Our data demonstrated that VA molecules bind in a small, well-defined, VDAC1 pocket comprising β-strands 14–16 and the distal part of the N-terminal helix does not involve the highly mobile residue K20, which is important for NADH binding.[29] The SC18 molecule, a recent discovery referenced in literature,[36] shares a similar region with VA molecules, although its precise binding site remains undefined. In contrast to SC18, VA molecules are marginally larger but lack nitro groups, which are generally considered toxic.[37]

VA molecules selectively kill cancer cells

The small molecular weight of the VA molecules, the satisfaction of the Lipinski's rule of five (MW < 500 Da, LogP <5, Hydrogen Bond Donor (HBD) <5, and (Polar Surface Area (PSA) <140 Å^2),[38] together with their ability to interfere with VDAC1 NADH binding and N-terminal helix movement, prompted us to test whether VA molecules can be effectively used to halt cancer cell proliferation.

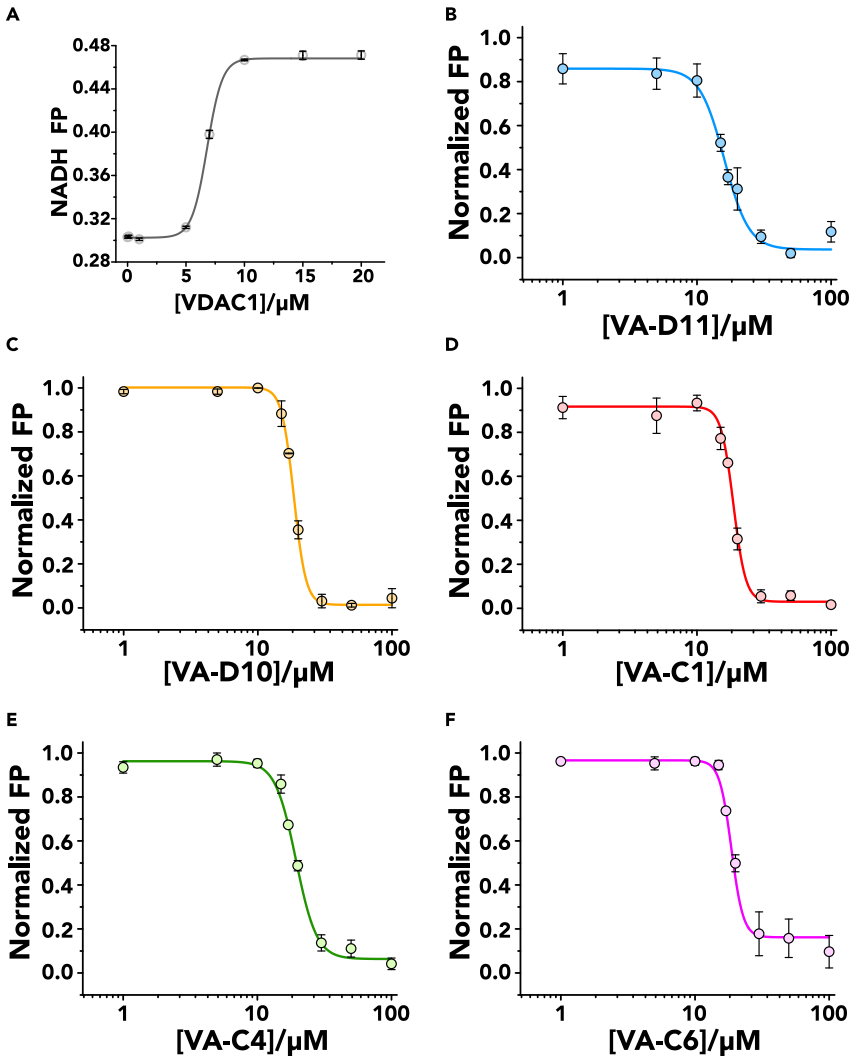

Figure 3. Direct binding of VA molecules to VDAC1 revealed by fluorescence polarization competition assay

(A) Binding of the NADH (at 5 μM) to increasing concentrations of mVDAC1 measured by fluorescence polarization (FP). 7 μM is the protein concentration used in all experiments.

(B–F) Displacement curves of the NADH (5 μM) from mVDAC1 with increased concentrations of VA-molecules. All the five molecules are able to compete with NADH binding with an apparent K_D in the micromolar range (K_DVA-D11 = 15.9 ± 0.6, K_DVA-D10 = 18.5 ± 0.2, K_DVA-C1 = 18.7 ± 0.3, K_DVA-C4 = 19.4 ± 0.4, K_DVA-C6 = 18.7 ± 0.5). Data are expressed as mean ± SEM (n = 3).

We initially tested the five selected molecules on the highly aggressive, highly glycolytic, breast cancer cell line SKBR3. All VA molecules show a marked reduction (~75% at VA high dose) in cell viability after 48 h of treatment. In the same set of experiments, the non-tumorigenic fibroblast cell line NIH-3T3 was not affected by the treatment (Figures 6A–6E). Notably, SKBR3 cells show increased level of VDAC1 protein expression compared to NIH-3T3 (Figure S3A). The calculated EC_{50} aligns with the K_D values found on the binding assays performed on the purified VDAC1 (Figure 6F), confirming that the effect is specific to VDAC1.

SKBR3 and NIH-3T3 are, however, commercial immortalized cell lines that hardly reproduce the tumor environment. To validate the effectiveness of the VA molecules as potential cancer treatment, we tested the molecules on primary cells derived from intrahepatic cholangiocarcinoma patients (iCCA) and on paired non-tumor liver cells, having a different expression level of VDAC1 (Figure S3B). Out of the five molecules, VA-C1, VA-D10, and VA-C4 show a similar reduction in iCCA cell viability of about 50% after 72 h of exposure to 2μM concentration of molecules (Figure 6G). Again, control cells were unaffected by the treatment (Figure 6G), underlining the ability of VA molecules to kill the cancer cells.

VDAC1-mediated disruption of NADH balance impairs mitochondrial function in glycolytic tumors

Given that (1) NADH crosses the OMM through VDAC1,[39] (2) VDAC1 is overexpressed in many tumor cells lines[40] including iCCA and SKBR3 (Figure S3) and (3) the SC18 molecule targeting the VDAC1 NADH binding site[36] reduces mitochondrial NADH, we hypothesized that VA molecules

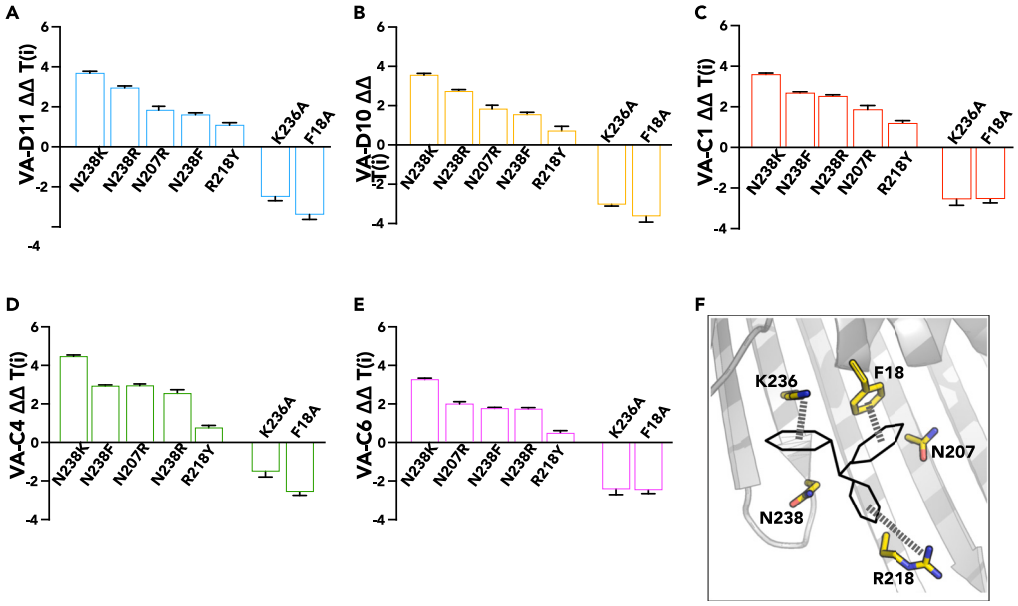

Figure 4. Identification of VA molecules framing residues

(A–E) ΔΔ inflection temperatures ($\Delta\Delta T_i$) values were obtained by subtracting the ΔT_i of mVDAC1 mutants from the ΔT_i of wild-type protein. Positive or negative $\Delta\Delta T_i$ values show the effect of stabilizing and destabilizing mutations on inflection temperature after treatment with VA molecules, respectively. Data are expressed as mean ± SEM (n = 3).

(F) Schematic representation of the V-shaped VA compounds and the interactions between VDAC1 residues and the three aromatic rings of the molecules. The thermal denaturation assays confirmed that a cation-π interaction between K236 and VA-L rings and a π−π stack between F18 and VA-R rings are essential for binding. The binding can be further improved by introducing additional π interactions in the neighboring residues.

can similarly impact mitochondrial energy generation by blocking the NADH transport. To test the hypothesis, we analyzed the oxygen consumption rate linked to OXPHOS in SKBR3 and NIH3T3cells by high-resolution respirometry (HRR). Figure S6 shows a representative respirometry curve of untreated NIH-3T3 and the specific protocol used. We first analyzed the OXPHOS respiration relative to the NADH electron transport pathway (N-pathway) driven by Complex I. This state was achieved in the presence of a combination of NADH-generating substrates (pyruvate, malate and glutamate) and saturating concentration of ADP, after a mild permeabilization of the plasma membranes. Then, the addition of succinate allowed the activation of Complex II and the measurement of the succinate pathway in combination with the N-pathway (NS-pathway).

Oxygen consumption corresponding to the reported respiratory states in cells treated with 10 μM of VA molecules for 48 h was monitored and compared to the control. As shown (Figure 7A; Table S2), a dramatic reduction of oxygen flows was detected in both N-pathway and NS-pathway, ranging from 15% to 40% in tumoral cell lines. Otherwise, in the same set of experiments, the NIH3T3cells were unaffected by the small molecule treatment. According to previous data, the net OXPHOS fluxes, corresponding to the oxygen consumption directly devoted to the ADP phosphorylation, were similarly reduced (Figure 7B).

Overall, these results indicate that the VA molecules can affect mitochondrial functionality only in high glycolytic cell lines, supporting their use as a potential therapeutic intervention for cancer treatment.

Establishment of organoid cultures for VA molecules testing

In order to verify the efficiency of VA molecules treatment in a reliable tumor-like context, we developed a suitable three-dimensional system of organoids from patients undergoing diagnostic surgical resection for iCCA.

Table 1. Inflection temperature (T[i]) values

	WT	*N238K*	*N238F*	*N238R*	*R218Y*	*N207R*	*K236A*	*F18A*
VA-D11	60.2 ± 0.1	64.5 ± 0.1	63.1 ± 0.1	63.1 ± 0.1	62.3 ± 0.1	62.9 ± 0.1	57.9 ± 0.1	57.2 ± 0.1
VA-D10	60.5 ± 0.1	64.4 ± 0.1	63.3 ± 0.1	63.1 ± 0.1	62.2 ± 0.2	62.9 ± 0.1	57.9 ± 0.1	57.3 ± 0.1
VA-C1	60.2 ± 0.1	64.0 ± 0.1	64.0 ± 0.1	62.5 ± 0.1	62.3 ± 0.1	63.2 ± 0.1	57.3 ± 0.1	58.0 ± 0.1
VA-C4	59.2 ± 0.1	64.0 ± 0.1	63.3 ± 0.1	61.6 ± 0.1	60.8 ± 0.1	63.0 ± 0.1	57.1 ± 0.1	57.9 ± 0.1
VA-C6	60.2 ± 0.1	63.8 ± 0.1	63.2 ± 0.1	61.8 ± 0.1	61.6 ± 0.1	63.0 ± 0.1	57.0 ± 0.1	58.1 ± 0.1

The table shows the T(i) [°C] values of the recombinant proteins mVDAC1 wild-type (WT) and mutants treated with the different small molecules at the final concentration of 1 mM in DMF. Data are reported as mean ± SEM of n = 3 independent experiments.

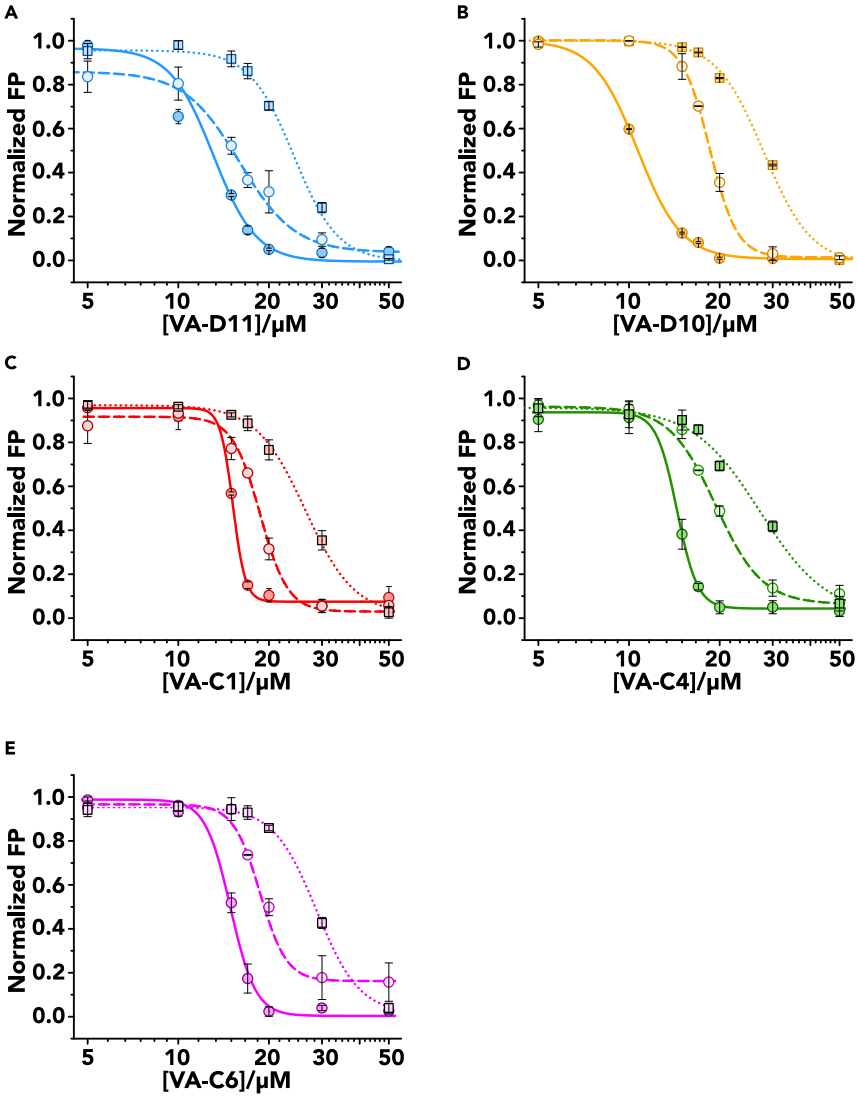

Figure 5. VDAC1 mutants affect VA molecule binding

(A–E) VA-induced NADH Fluorescence polarization displacement curves from mVDAC1 wild-type (dashed lines) and stabilizing (mVDAC1 N238K—solid line) or destabilizing (mVDAC1 K236A—dotted lines) mutants with increasing concentrations of VA-molecules. K236A and N238K shows decreased and increased affinity, respectively compared to the wild-type channel (K_DVA-D11$_{KA}$ = 24.2 ± 0.6, K_DVA-D10$_{KA}$ = 28.0 ± 0.7, K_DVA-C1$_{KA}$ = 26.4 ± 0.4, K_DVA-C4$_{KA}$ = 27 ± 1, K_DVA-C6$_{KA}$ = 28.8 ± 0.2; K_DVA-D11$_{NK}$ = 13.1 ± 0.4, K_DVA-D10$_{NK}$ = 10.7 ± 0.1, K_DVA-C1$_{NK}$ = 15.20 ± 0.04, K_DVA-C4$_{NK}$ = 14.4 ± 0.2, K_DVA-C6 $_{NK}$ = 14.9 ± 0.5). Experiments were performed using a final protein concentration of 7 μM. Data are expressed as mean ± SEM (n = 3). (See also Figure S2).

Organoids were obtained from both iCCA and non-tumor tissues in 5 of the 6 patients included in the study, considering our cohort's underlying disease spectrum (Table S3).

Tumor organoids allowed long-term *in vitro* expansion, in contrast with organoids derived from non-tumor tissues, which showed a more robust proliferation at the early stage of culture, but after a few months stopped to proliferate. Organoids morphologically showed a cystic structure, with an external layer that defined an internal core (Figure S4A), features that have described.[41]

Further, we characterized the organoids by immunofluorescence technique to map the presence of molecular markers, attesting their reliability for drug testing. We revealed the expression of typical biliary markers, such as epithelial cell adhesion molecule (EpCaM), cytokeratin 7 (CK7), and cytokeratin 19 (CK19) (Figure S4B). Moreover, we analyzed the level of nuclear antigen Ki67 in tumor organoids, confirming that its presence >5% is an important requirement for successful organoid derivation (Figure S4B).[42]

RT-PCR performed on iCCA cells compared to non-tumor cells showed overexpression of VDAC1 mRNA exclusively in cancer cells (Figure S3B), leading us to use this system to test the effect of VA molecules on 3D cultures.

Table 2. Kd values in NADH—VA-molecules competition assay

	WT	*N238K*	*K236A*
VA-D11	15.9 ± 0.7	13.1 ± 0.4	24.2 ± 0.6
VA-D10	18.5 ± 0.2	10.7 ± 0.1	28.0 ± 0.7
VA-C1	18.7 ± 0.3	15.2 ± 0.1	26.4 ± 0.4
VA-C4	19.4 ± 0.4	14.4 ± 0.2	27.2 ± 1.5
VA-C6	18.7 ± 0.6	14.9 ± 0.5	28.8 ± 0.2

In table are reported the Kd values (expressed in μM) obtain after FP assays. Stabilized and destabilized mutant (N238K and K236A) show a variation in affinity with VA-molecules compere to wild-type protein, increase or decrease, respectively. Data are expressed as mean ± SEM of $n = 3$ independent experiments.

Organoids are valid pre-clinical models to test VA molecules efficacy

The absence of appropriate *in vitro* models that accurately represent the cancer biology and heterogeneity of patients is a significant barrier to the development of new therapies and biomarkers for iCCA. Liver organoids can represent an ideal approach due to their ability to retain the morphological properties of primary tissue and to assess different biological features, including proliferation, signaling, and cell-cell interaction.[43]

Based on this premise, we tested the impact of different dosages of VA molecules both in iCCA and non-tumor organoid cultures, monitoring cell viability after 72 h. In these *in vitro* assays, we observed that VA molecules treatment selectively decreased iCCA-derived organoids growth in a dose-dependent manner, with an EC_{50} of 25 ± 6, 15 ± 2 and 19 ± 1 μM for VA-D10, VA-C1 and VA-C4, respectively (Figure 8). Strikingly we measured a very low effect on the viability of non-tumor cells. In addition, we compared *in vitro* VA molecules activity with the gemcitabine (GMB), clinically used for iCCA treatment. GMB demonstrates significant efficacy against both iCCA and control organoids, even at concentrations five times lower than those of VA molecules (Figure S5). This underscores the enhanced chemical potency of VA molecules compared to standard drugs.

Taken together, these results demonstrate that selectively displacing NADH from VDAC1 cavity hampers cancer cell survival and show the first evidence that chemical entities specifically targeting the major mitochondrial porin are effective on patient-derived tumor primary cells, paving the way for the development of precision medicine VDAC1-targeted drugs.

DISCUSSION

Small molecule modulation of cell fate is one of the major research areas in cancer biology, but it is still one of the most challenging. Cancer research, indeed, must face the heterogeneity of cancer phenotypes, the individual immune response to the disease[44] and the general cytotoxicity of chemotherapeutics.[45] These challenges necessitate efforts to develop specific anticancer agents. The long process from bench research to clinical trials additionally slows down the generation of novel classes of molecules.

Targeting cancer metabolism as a universal strategy has been proposed for years. However, most of the efforts have been directed toward either inhibiting enzymes involved in the glycolysis[46] or impairing the mitochondrial activity,[47] strategies based on the high glycolytic activity of certain cancer types or on the mitochondrial dysfunction of others. A unique molecule capable of playing on both sides is still elusive.

Rather than just a mere ion channel, VDAC1 figures as a molecular switch for the modulation of the cell bioenergetics and links glycolysis to mitochondrial metabolism by its direct interaction with HKs. Except for some compensatory effect given by other isoforms, the inactivation of VDAC1 gene triggers a re-arrangement of the electron transport system functioning.[48,49] Therefore, targeting the major mitochondrial metabolite transporter VDAC1 could represent a promising strategy since the channel is involved in many cancer processes, i.e., the inhibition of apoptosis, and it is considered the "mitochondrial gate keeper" because of its role in metabolite translocation from the cytosol to the mitochondria and vice-versa. However, most of the identified molecules are either not specific, with undesired side effects on channel function, or biochemically poorly characterized,[19,32,50,51] lowering the chances for a further pharmaceutical development. A number of agents have been employed to disrupt the HK-VDAC1 complex (clotrimazole or 3-bromopyruvate),[52] inhibit VDAC1 conductance (DIDS and derivatives)[53] or reduce VDAC1 expression.[18,21,22] However, for many of them the effect was not limited on cancer cells but it was also registered in normal tissues, especially those that use glucose as the main energy source.[54]

In light of these considerations, we rationalized that a binding pocket away from VDAC1 central cavity would be the ideal spot for small molecules modulation. This region seems to be shared by the recently discovered SC18 molecule,[36] even though its exact binding pocket has not been uniquely identified. Following our *in silico* results, we developed a workflow to test these small molecules targeting VDAC1 using a combination of direct binding detection on the purified target and further validation on patient-derived primary cell cancer organoids. Using a bottle-neck strategy, we identified three drug-like candidates that perform well on cholangiocarcinoma organoids and adherent cancer cell models, but at the same time they leave unperturbed healthy cells and organoids. VA molecules are slightly bigger than SC18, but on the contrary they do not present nitro-groups, which are often considered toxic.[37] Both SC18 and VA molecules have shown inhibitory effects on cancer cell viability in 2D cultures, yet VA molecules act significantly faster, achieving up to 75% inhibition in 48 h. This rapid efficacy extends to patient-derived cancer cells, where a 50% decrease in cell viability occurs within the same time frame at lower concentrations (2uM). SC18 requires 4-5 days to achieve similar outcomes.[36] Compared to other synthetic molecules targeting VDAC1 (i.e., VBIT-3/4),[50] VA molecules are significantly smaller (average number of atoms is 39 and 52 for VA and VBIT molecules, respectively).

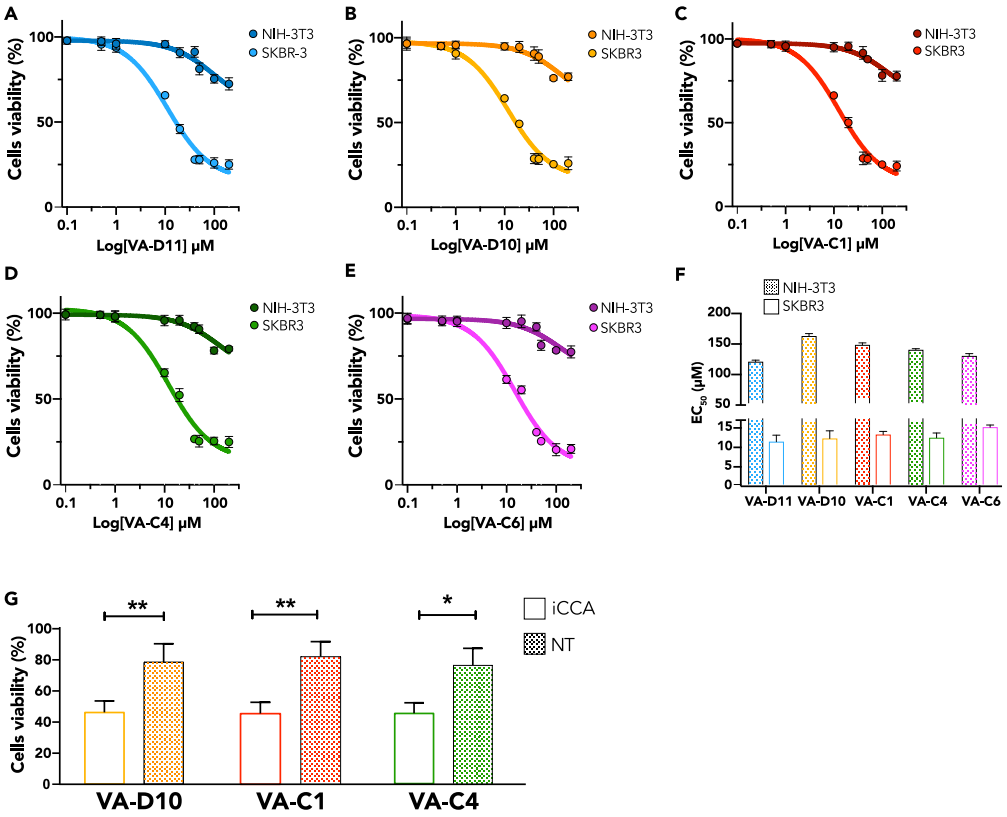

Figure 6. VA molecules affect the viability of cancer cells

(A–F) Dose-response curves representing cell viability of NIH-3T3 and SKBR-3 treated with different concentrations of VA molecules (VA-D11, VA-D10, VA-C1, VA-C4, and VA- C6). Data are expressed as mean ± SEM ($n = 3$). (F) Bar plot reporting Half the effective dose (EC_{50}) retrieved after cell viability assay. SKBR-3 cell lines show greater sensitivity to treatment with the five molecules (VA-D11: 10 ± 2 μM; VA-D10 10 ± 1 μM; VA-C1 11 ± 2 μM; VA-C4 11 ± 3 μM; VA-C6 10 ± 2 μM) then NIH3T3cell lines (VA-D11: 118 ± 3 μM; VA-D10 160 ± 4 μM; VA-C1 146 ± 3 μM; VA-C4 137 ± 2 μM; VA-C6 127 ± 4 μM).

(G) The effect of VA molecules (D10, C1, C4) on the viability of iCCA patient-derived and paired non-tumor (NT) 2D cells. Viability was measured by MTT assay after 72 h exposure using 2μM concentration (*$p < 0,05$, **$p < 0,01$). Data are represented as mean ± SEM ($n = 3$). (See also Figure S3).

The computational and biochemical characterization of VA molecules revealed a binding site framed by five residues, Phe18, Asn207, Arg218, Lys236, and Asn238, within the α-helix/β-barrel interface, revealing a pocket partly shared by NADH. The competition for the binding pocket suggests that, upon VA molecules binding and NADH displacement, no more NADH can cross the mitochondrial membrane. Given the effect on NADH on VDAC1 conductance,[30] it is reasonable to speculate that VA molecules can also impact VDAC1 channel gating. This aspect will need further investigation through electrophysiological characterization.

The NAD^+/NADH homeostasis is a key player in cancer cell survival because of its role in metabolic advantage for sustained cell proliferation.[55] The NAD^+ depletion through mutations in the isocitrate dehydrogenase genes has been shown to dramatically affect the mitochondrial TCA cycle and solid tumor vitality.[56] TCA cycle metabolites themselves are physiological signaling molecules[57] able to control anabolism, catabolism and cell fate. In highly glycolytic cancer cells (such as iCCA or the commercial breast cancer SKBR3 used in this study), the altered mitochondrial bioenergetics lead to uncontrolled proliferation and tumor progression. High lactate production, indeed, is oxidized back to pyruvate to foster TCA cycle. Therefore, a higher demand for NADH is required for the TCA cycle to proceed. Hence, limiting the NADH availability can slow down the mitochondrial electron transport capacity by directly influencing the Complex I (NADH ubiquinone-oxidoreductase) and indirectly the Complex II (succinate dehydrogenase) by limiting its own substrate.

As a matter of fact, HRR data showed a tremendous impact on mitochondrial respiration in our cancer cell model following treatment with molecules and, precisely, in the measurement achieved in the exclusive presence of NADH-linked substrates. These data suggest a significant reduction of the Complex I contribution to the OXPHOS respiration, possibly due to reduced NADH levels, which are normally established in the mitochondria by VDAC1 transport. The impact of VA molecules on respiration appears even more drastic considering that the further activation of Complex II by succinate cannot overcome the mitochondrial dysfunction. Indeed, the oxygen flows relative to the total OXPHOS respiration (NS-pathway and the ATP-related fluxes) are significantly lower in VA-treated cells compared to the untreated controls. Therefore, it could be hypothesized that the binding of these drugs would lead to a change in the translocation of NADH or other

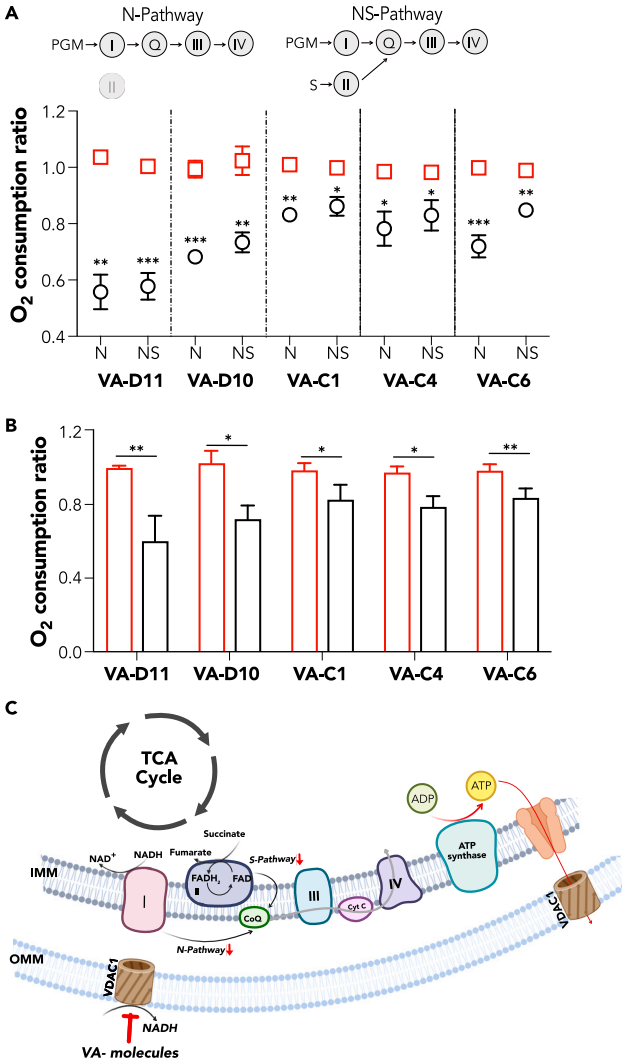

Figure 7. High-resolution respirometry shows cancer cell mitochondrial distress upon VA treatment

(A) Quantitative analysis of the oxygen consumption in the analyzed states (N-Pathway and NS-Pathway) of SKBR-3 and NIH-3T3 attained after the exposure to 10 μM VA-molecules for 48h. Data are indicated as the mean ± SEM (n = 3) and expressed as the ratio of the treated cells to the untreated ones. Data were analyzed by unpaired t-test, with *p < 0.05, **p < 0.01 and ***p < 0.001.

(B) Quantitative analysis of the net oxygen consumption in the NS-Pathway or ATP-linked flux of SKBR-3 and NIH-3T3 attained after the exposure to 10 μM VA-molecules for 48h. Data are indicated as the mean ± SEM (n = 3) and expressed as the ratio of the treated cells to the untreated ones. Data were analyzed by unpaired t-test, with *p < 0.05, **p < 0.01 and ***p < 0.001.

(C) Proposed mechanism for NADH imbalance through VDAC1. Panel C has been created with BioRender.com (See also Figure S6).

mitochondrial metabolites through the porin, causing an imbalance in the TCA cycle by limiting the cofactors necessary for the first respiratory chain reaction complex in which mitochondria respiration are affected.

The results are strengthened by the null effect of VA molecules on non-tumor cell lines. The expression of VDAC1 is increased in numerous human cancer cell lines compared to normal cell lines,[58–61] and this could explain the different impact observed on mitochondrial activity and cell proliferation observed. The strategy of using patient-derived organoids has been successful in recognizing only the small molecules that potentially would be effective *in vivo*, by excluding either some of the cell biology hits that were not effective on fibroblasts but were killing the organoids and all the compounds that were also killing the control organoids.

The identified compounds have an average EC_{50} in the micromolar range, therefore they cannot be directly used as therapeutics. However, we (1) have identified a precise hot-spot in VDAC1 that could be an easy target for additional drug-screening campaigns; (2) isolated three effective drug-like novel chemical entities that can be further optimized by simple medicinal chemistry and biochemical studies as reported; (3) designed a simple killing method using organoids that will boost the further drug development of these compounds since the animal models are not any longer required to proceed to clinical trials if scaffolded 3D cultures are used.[62]

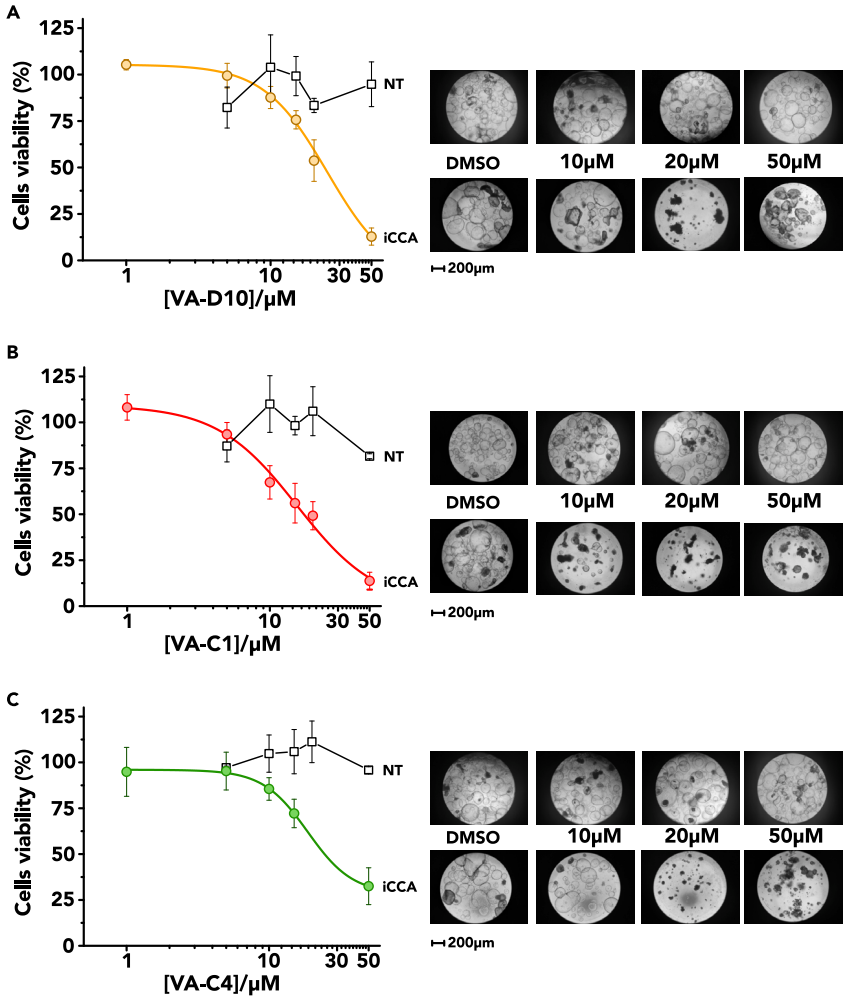

Figure 8. Cholangiocarcinoma 3D models are affected by VA treatment

Tumor (iCCA) and non-tumor (NT) organoids were exposed to VA treatment for 72 h at the indicated concentration. DMSO-treated organoids were used as control. (A–C) Left panel: VA treatment (D10, C1, C4) reduce cell viability of iCCA organoids in a dose-dependent manner, while show a limited effect on non-tumor organoids. Data are represented as the percentage of control DMSO-treated organoids and are the mean of at least three independent experiments ±SEM. Right panel: representative bright-field images of tumor and non-tumor organoids exposed to VA treatment (D10, C1, C4) at the indicated concentration for 72h. Scale bar: 200 μm. (See also Figures S4 and S5).

Limitations of the study

This study provides evidence that targeting the NADH binding site in VDAC1 with small molecules selectively impacts cancer organoids. However, it also acknowledges certain limitations. While our compounds showed promising results in patient-derived intrahepatic cholangiocarcinoma (iCCA) models, the applicability of VA molecules as a universal anti-cancer treatment is yet to be determined, necessitating further investigation across a broader spectrum of patient cohorts and cancer types. Additionally, this study did not assess the impact of these molecules on the electrophysiological properties of VDAC1 yet, whose gating plays a critical role in mitochondrial functionality. Thus, a dedicated mechanistic study will be essential to elucidate these effects comprehensively.

STAR★METHODS

Detailed methods are provided in the online version of this paper and include the following:

- KEY RESOURCES TABLE
- RESOURCE AVAILABILITY
  - Lead contact
  - Materials availability

SUPPLEMENTAL INFORMATION

Supplemental information can be found online at https://doi.org/10.1016/j.isci.2024.109853.

ACKNOWLEDGMENTS

We thank Dr. Jeff Abramson for kindly providing us with the plasmid pQE9 encoding the mouse VDAC1 gene. We are grateful to L. Iamele, and H. de Jonge, University of Pavia, Italy, for providing Human HGF/SF.[63]

We thank the core facility "Centro Grandi Strumenti" (CGS) at the University of Pavia for providing access to the Confocal Microscopy laboratory and technical support.

This work was supported by "Programma per Giovani Ricercatori—Rita Levi Montalcini 2016" granted by the Italian Ministry of Education (Project number: PGR16HTPSF), by the Department of Molecular Medicine of the University of Pavia, Italy under the initiative Dipartimenti di Eccellenza (2018–2022) and by the Cariplo Foundation (#2019-1809) to M.L; Immuno-HUB_T4-CN-02-anno 2021 to C.T.; PRIN 2022 PNRR E53D2302170 0001 (Funded by European Union—NextGeneration UE) to A.Magrì and PNRR M4C2-Investment 1.4- CN000041 (Funded by the European Union—NextGenerationEU) to V.D.P. and A. Messina. This work benefited of the support and the use of resources of Instruct-ERIC, and specifically of the CERM/CIRMMP Italy Centre (PID: 25293 to M.L.). Atomwise Inc. performed the virtual screening, provided the compounds, and managed their delivery through the Atomwise AIMS Award (A19-314) to M.L.

AUTHOR CONTRIBUTIONS

C.A., C.T., and M.L. conceived the study and designed the experiments. S.C.N., S.D.S., E.L., and A. Magrì performed the experiments. S.C.N. performed protein expression and purification experiments, fluorescence polarization and thermostability assays, viability assays on commercial cells lines, and analyzed the data. S.D.S. performed the cell culture experiments on patient-derived cells and organoids and analyzed the data. E.L. performed NMR experiments. A. Magrì. and S.C.N. performed the high-resolution respirometry (HRR) experiments and analyzed the data together with A. Messina. M.U.M., S.M., and B.O. provided patients biopsies. L.B. supervised the HRR experiments. C.A., C.T., V.D.P., and M.L. analyzed the data and provided guidance and support throughout.

S.C.N., S.D.S., E.L., A.Magrì., M.U.M., S.M., B.O., V.D.P., C.T., C.A., and M.L. wrote the paper.

DECLARATION OF INTERESTS

The authors declare no competing interests.

Received: November 23, 2023
Revised: March 6, 2024
Accepted: April 26, 2024
Published: April 30, 2024

REFERENCES

1. Dang, C.V., and Kim, J.-W. (2018). Convergence of cancer metabolism and immunity: an overview. Biomol. Ther. *26*, 4–9.
2. DeBerardinis, R.J., and Chandel, N.S. (2016). Fundamentals of cancer metabolism. Sci. Adv. *2*, e1600200.
3. Messina, A., Reina, S., Guarino, F., and De Pinto, V. (2012). VDAC isoforms in mammals. Biochim. Biophys. Acta *1818*, 1466–1476.
4. Camara, A.K.S., Zhou, Y., Wen, P.-C., Tajkhorshid, E., and Kwok, W.-M. (2017). Mitochondrial VDAC1: a key gatekeeper as potential therapeutic target. Front. Physiol. *8*, 460.
5. Tsujimoto, Y., and Shimizu, S. (2000). VDAC regulation by the Bcl-2 family of proteins. Cell Death Differ. *7*, 1174–1181.
6. Magrì, A., Risiglione, P., Caccamo, A., Formicola, B., Tomasello, M.F., Arrigoni, C., Zimbone, S., Guarino, F., Re, F., and Messina, A. (2021). Small hexokinase 1 peptide against toxic SOD1 G93A mitochondrial accumulation in ALS rescues the ATP-related respiration. Biomedicines *9*, 948.
7. Haloi, N., Wen, P.-C., Cheng, Q., Yang, M., Natarajan, G., Camara, A.K.S., Kwok, W.-M., and Tajkhorshid, E. (2021). Structural basis of complex formation between mitochondrial anion channel VDAC1 and Hexokinase-II. Commun. Biol. *4*, 667.
8. Vyssokikh, M.Y., and Brdiczka, D. (2003). The function of complexes between the outer mitochondrial membrane pore (VDAC) and the adenine nucleotide translocase in regulation of energy metabolism and apoptosis. Acta Biochim. Pol. *50*, 389–404.
9. Fang, Y., Liu, J., Zhang, Q., She, C., Zheng, R., Zhang, R., Chen, Z., Chen, C., and Wu, J. (2022). Overexpressed VDAC1 in breast cancer as a novel prognostic biomarker and correlates with immune infiltrates. World J. Surg. Oncol. *20*, 211.
10. Pittala, S., Krelin, Y., and Shoshan-Barmatz, V. (2018). Targeting liver cancer and associated pathologies in mice with a mitochondrial VDAC1-based peptide. Neoplasia *20*, 594–609.
11. Zhang, G., Jiang, G., Wang, C., Zhong, K., Zhang, J., Xue, Q., Li, X., Jin, H., and Li, B. (2016). Decreased expression of microRNA-320a promotes proliferation and invasion of non-small cell lung cancer cells by increasing VDAC1 expression. Oncotarget *7*, 49470–49480.
12. Gao, W., Xua, J., Wang, F., Zhang, L., Peng, R., Zhu, Y., Tang, Q., and Wu, J. (2015). Mitochondrial proteomics approach reveals voltage-dependent anion channel 1 (VDAC1) as a potential biomarker of gastric cancer. Cell. Physiol. Biochem. *37*, 2339–2354.
13. Wang, W., Zhang, T., Zhao, W., Xu, L., Yang, Y., Liao, Q., and Zhao, Y. (2016). A single talent immunogenic membrane antigen and novel prognostic predictor: voltage-dependent anion channel 1 (VDAC1) in pancreatic cancer. Sci. Rep. *6*, 33648.
14. Pedersen, P.L. (2008). Voltage dependent anion channels (VDACs): a brief introduction with a focus on the outer mitochondrial compartment's roles together with hexokinase-2 in the "Warburg effect" in cancer. J. Bioenerg. Biomembr. *40*, 123–126.
15. Shoshan-Barmatz, V., and Golan, M. (2012). Mitochondrial VDAC1: function in cell life and death and a target for cancer therapy. Curr. Med. Chem. *19*, 714–735.
16. Shoshan-Barmatz, V., Ben-Hail, D., Admoni, L., Krelin, Y., and Tripathi, S.S. (2015). The mitochondrial voltage-dependent anion channel 1 in tumor cells. Biochim. Biophys. Acta *1848*, 2547–2575.
17. Mazure, N.M. (2017). VDAC in cancer. Biochim. Biophys. Acta Bioenerg. *1858*, 665–673.
18. Reina, S., and De Pinto, V. (2017). Anti-cancer compounds targeted to VDAC: potential and perspectives. Curr. Med. Chem. *24*, 4447–4469.
19. Magri, A., Reina, S., and De Pinto, V. (2018). VDAC1 as pharmacological target in cancer and neurodegeneration: focus on its role in apoptosis. Front. Chem. *6*, 108.
20. Tewari, D., Majumdar, D., Vallabhaneni, S., and Bera, A.K. (2017). Aspirin induces cell death by directly modulating mitochondrial voltage-dependent anion channel (VDAC). Sci. Rep. *7*, 45184.
21. Freitas, S., Martins, R., Costa, M., Leão, P.N., Vitorino, R., Vasconcelos, V., and Urbatzka, R. (2016). Hierridin B isolated from a marine cyanobacterium alters VDAC1, mitochondrial activity, and cell cycle genes on HT-29 colon adenocarcinoma cells. Mar. Drugs *14*, 158.
22. Huang, L., Han, J., Ben-Hail, D., He, L., Li, B., Chen, Z., Wang, Y., Yang, Y., Liu, L., Zhu, Y., et al. (2015). A New Fungal Diterpene Induces VDAC1-dependent Apoptosis in Bax/Bak-deficient Cells. J. Biol. Chem. *290*, 23563–23578.
23. Wei, L., Zhou, Y., Dai, Q., Qiao, C., Zhao, L., Hui, H., Lu, N., and Guo, Q.L. (2013). Oroxylin A induces dissociation of hexokinase II from the mitochondria and inhibits glycolysis by SIRT3-mediated deacetylation of cyclophilin D in breast carcinoma. Cell Death Dis. *4*, e601.
24. Yuan, S., Fu, Y., Wang, X., Shi, H., Huang, Y., Song, X., Li, L., Song, N., and Luo, Y. (2008). Voltage-dependent anion channel 1 is involved in endostatin-induced endothelial cell apoptosis. FASEB J. *22*, 2809–2820.
25. Penso, J., and Beitner, R. (1998). Clotrimazole and bifonazole detach hexokinase from mitochondria of melanoma cells. Eur. J. Pharmacol. *342*, 113–117.
26. Nakashima, R.A. (1989). Hexokinase-binding properties of the mitochondrial VDAC protein: inhibition by DCCD and location of putative DCCD-binding sites. J. Bioenerg. Biomembr. *21*, 461–470.
27. Colombini, M., Yeung, C.L., Tung, J., and König, T. (1987). The mitochondrial outer membrane channel, VDAC, is regulated by a synthetic polyanion. Biochim. Biophys. Acta *905*, 279–286.
28. Nakashima, R.A., Mangan, P.S., Colombini, M., and Pedersen, P.L. (1986). Hexokinase receptor complex in hepatoma mitochondria: evidence from N,N′-dicyclohexylcarbodiimide-labeling studies for the involvement of the pore-forming protein VDAC. Biochemistry *25*, 1015–1021.
29. Bohm, R., Amodeo, G.F., Murlidaran, S., Chavali, S., Wagner, G., Winterhalter, M., Brannigan, G., and Hiller, S. (2020). The structural basis for low conductance in the membrane protein VDAC upon beta-NADH binding and voltage gating. Structure *28*, 206–214.
30. Zizi, M., Forte, M., Blachly-Dyson, E., and Colombini, M. (1994). NADH regulates the gating of VDAC, the mitochondrial outer membrane channel. J. Biol. Chem. *269*, 1614–1616.
31. Najbauer, E.E., Tekwani Movellan, K., Giller, K., Benz, R., Becker, S., Griesinger, C., and Andreas, L.B. (2022). Structure and gating behavior of the human integral membrane protein VDAC1 in a lipid bilayer. J. Am. Chem. Soc. *144*, 2953–2967.
32. Manzo, G., Serra, I., Magrí, A., Casu, M., De Pinto, V., Ceccarelli, M., and Scorciapino, M.A. (2018). Folded structure and membrane affinity of the N-terminal domain of the three human isoforms of the mitochondrial voltage-dependent anion-selective channel. ACS Omega *3*, 11415–11425.
33. Huynh, K., and Partch, C.L. (2015). Analysis of protein stability and ligand interactions by thermal shift assay. Curr. Protoc. Protein Sci. *79*, 28.9.1–28.9.14.
34. Dalvit, C., and Vulpetti, A. (2019). Ligand-based fluorine NMR screening: principles and applications in drug discovery projects. J. Med. Chem. *62*, 2218–2244.
35. Buchholz, C.R., and Pomerantz, W.C.K. (2021). (19)F NMR viewed through two different lenses: ligand-observed and protein-observed (19)F NMR applications for fragment-based drug discovery. RSC Chem. Biol. *2*, 1312–1330.
36. Heslop, K.A., Burger, P., Kappler, C., Solanki, A.K., Gooz, M., Peterson, Y.K., Mills, C., Benton, T., Duncan, S.A., Woster, P.M., and Maldonado, E.N. (2022). Small molecules targeting the NADH-binding pocket of VDAC modulate mitochondrial metabolism in hepatocarcinoma cells. Biomed. Pharmacother. *150*, 112928.
37. Nepali, K., Lee, H.Y., and Liou, J.P. (2019). Nitro-group-containing drugs. J. Med. Chem. *62*, 2851–2893.
38. Lipinski, C.A., Lombardo, F., Dominy, B.W., and Feeney, P.J. (2001). Experimental and computational approaches to estimate solubility and permeability in drug discovery and development settings. Adv. Drug Deliv. Rev. *46*, 3–26.
39. Shoshan-Barmatz, V., De Pinto, V., Zweckstetter, M., Raviv, Z., Keinan, N., and Arbel, N. (2010). VDAC, a multi-functional mitochondrial protein regulating cell life and death. Mol. Aspects Med. *31*, 227–285.
40. Wang, Z., Cheng, Y., Song, Z., and Zhao, R. (2022). Pan-cancer analysis of voltage-dependent anion channel (VDAC1) as a cancer therapeutic target or diagnostic biomarker. Dis. Markers *2022*, 5946110.
41. Saito, Y., Muramatsu, T., Kanai, Y., Ojima, H., Sukeda, A., Hiraoka, N., Arai, E., Sugiyama, Y., Matsuzaki, J., Uchida, R., et al. (2019). Establishment of patient-derived organoids and drug screening for biliary tract carcinoma. Cell Rep. *27*, 1265–1276.e4.
42. Nuciforo, S., Fofana, I., Matter, M.S., Blumer, T., Calabrese, D., Boldanova, T., Piscuoglio, S., Wieland, S., Ringnalda, F., Schwank, G., et al. (2018). Organoid models of human liver cancers derived from tumor needle biopsies. Cell Rep. *24*, 1363–1376.
43. De Siervi, S., and Turato, C. (2023). Liver Organoids as an *in vitro* model to study primary liver cancer. Int. J. Mol. Sci. *24*, 4529.
44. De Palma, M., and Hanahan, D. (2012). The biology of personalized cancer medicine: facing individual complexities underlying hallmark capabilities. Mol. Oncol. *6*, 111–127.
45. Fu, B., Wang, N., Tan, H.Y., Li, S., Cheung, F., and Feng, Y. (2018). Multi-component herbal

products in the prevention and treatment of chemotherapy-associated toxicity and side effects: a review on experimental and clinical evidences. Front. Pharmacol. *9*, 1394.
46. Pelicano, H., Martin, D.S., Xu, R.H., and Huang, P. (2006). Glycolysis inhibition for anticancer treatment. Oncogene *25*, 4633–4646.
47. Zong, W.X., Rabinowitz, J.D., and White, E. (2016). Mitochondria and cancer. Mol. Cell *61*, 667–676.
48. Magri, A., Cubisino, S.A.M., Battiato, G., Lipari, C.L.R., Conti Nibali, S., Saab, M.W., Pittala, A., Amorini, A.M., De Pinto, V., and Messina, A. (2023). VDAC1 knockout affects mitochondrial oxygen consumption triggering a rearrangement of ETC by impacting on complex I activity. Int. J. Mol. Sci. *24*, 3687.
49. Magri, A., Di Rosa, M.C., Orlandi, I., Guarino, F., Reina, S., Guarnaccia, M., Morello, G., Spampinato, A., Cavallaro, S., Messina, A., et al. (2020). Deletion of Voltage-Dependent Anion Channel 1 knocks mitochondria down triggering metabolic rewiring in yeast. Cell. Mol. Life Sci. *77*, 3195–3213.
50. Ben-Hail, D., Begas-Shvartz, R., Shalev, M., Shteinfer-Kuzmine, A., Gruzman, A., Reina, S., De Pinto, V., and Shoshan-Barmatz, V. (2016). Novel compounds targeting the mitochondrial protein VDAC1 inhibit apoptosis and protect against mitochondrial dysfunction. J. Biol. Chem. *291*, 24986–25003.
51. Liu, Y., Cheng, H., Zhou, Y., Zhu, Y., Bian, R., Chen, Y., Li, C., Ma, Q., Zheng, Q., Zhang, Y., et al. (2013). Myostatin induces mitochondrial metabolic alteration and typical apoptosis in cancer cells. Cell Death Dis. *4*, e494.
52. Krasnov, G.S., Dmitriev, A.A., Lakunina, V.A., Kirpiy, A.A., and Kudryavtseva, A.V. (2013). Targeting VDAC-bound hexokinase II: a promising approach for concomitant anti-cancer therapy. Expert Opin. Ther. Targets *17*, 1221–1233.
53. Ben-Hail, D., and Shoshan-Barmatz, V. (2016). VDAC1-interacting anion transport inhibitors inhibit VDAC1 oligomerization and apoptosis. Biochim. Biophys. Acta *1863*, 1612–1623.
54. Shoshan-Barmatz, V., Krelin, Y., Shteinfer-Kuzmine, A., and Arif, T. (2017). Voltage-dependent anion channel 1 as an emerging drug target for novel anti-cancer therapeutics. Front. Oncol. *7*, 154.
55. Moreira, J.D.V., Hamraz, M., Abolhassani, M., Bigan, E., Pérès, S., Paulevé, L., Nogueira, M.L., Steyaert, J.M., and Schwartz, L. (2016). The redox status of cancer cells supports mechanisms behind the warburg effect. Metabolites *6*, 33.
56. Tateishi, K., Wakimoto, H., Iafrate, A.J., Tanaka, S., Loebel, F., Lelic, N., Wiederschain, D., Bedel, O., Deng, G., Zhang, B., et al. (2015). Extreme vulnerability of IDH1 mutant cancers to NAD^+ depletion. Cancer Cell *28*, 773–784.
57. Martinez-Reyes, I., and Chandel, N.S. (2020). Mitochondrial TCA cycle metabolites control physiology and disease. Nat. Commun. *11*, 102.
58. Shinohara, Y., Ishida, T., Hino, M., Yamazaki, N., Baba, Y., and Terada, H. (2000). Characterization of porin isoforms expressed in tumor cells. Eur. J. Biochem. *267*, 6067–6073.
59. Simamura, E., Hirai, K.I., Shimada, H., Koyama, J., Niwa, Y., and Shimizu, S. (2006). Furanonaphthoquinones cause apoptosis of cancer cells by inducing the production of reactive oxygen species by the mitochondrial voltage-dependent anion channel. Cancer Biol. Ther. *5*, 1523–1529.
60. Simamura, E., Shimada, H., Hatta, T., and Hirai, K.I. (2008). Mitochondrial voltage-dependent anion channels (VDACs) as novel pharmacological targets for anti-cancer agents. J. Bioenerg. Biomembr. *40*, 213–217.
61. Shoshan-Barmatz, V., and Ben-Hail, D. (2012). VDAC, a multi-functional mitochondrial protein as a pharmacological target. Mitochondrion *12*, 24–34.
62. Wadman, M. (2023). FDA no longer has to require animal testing for new drugs. Science *379*, 127–128.
63. de Nola, G., Leclercq, B., Mougel, A., Taront, S., Simonneau, C., Forneris, F., Adriaenssens, E., Drobecq, H., Iamele, L., Dubuquoy, L., et al. (2022). Dimerization of kringle 1 domain from hepatocyte growth factor/scatter factor provides a potent MET receptor agonist. Life Sci. Alliance *5*, e202201424.
64. Gherardi, E., Sandin, S., Petoukhov, M.V., Finch, J., Youles, M.E., Ofverstedt, L.G., Miguel, R.N., Blundell, T.L., Vande Woude, G.F., Skoglund, U., and Svergun, D.I. (2006). Structural basis of hepatocyte growth factor/scatter factor and MET signalling. Proc. Natl. Acad. Sci. USA *103*, 4046–4051.
65. Reina, S., Nibali, S.C., Tomasello, M.F., Magrì, A., Messina, A., and De Pinto, V. (2022). Voltage dependent anion channel 3 (VDAC3) protects mitochondria from oxidative stress. Redox Biol. *51*, 102264.
66. Ujwal, R., Cascio, D., Colletier, J.P., Faham, S., Zhang, J., Toro, L., Ping, P., and Abramson, J. (2008). The crystal structure of mouse VDAC1 at 2.3 A resolution reveals mechanistic insights into metabolite gating. Proc. Natl. Acad. Sci. USA *105*, 17742–17747.
67. O'Boyle, N.M., Banck, M., James, C.A., Morley, C., Vandermeersch, T., and Hutchison, G.R. (2011). Open Babel: An open chemical toolbox. J. Cheminform. *3*, 33.
68. Eberhardt, J., Santos-Martins, D., Tillack, A.F., and Forli, S. (2021). AutoDock Vina 1.2.0: new docking methods, expanded force field, and python bindings. J. Chem. Inf. Model. *61*, 3891–3898.
69. Atomwise AIMS Program (2024). AI is a viable alternative to high throughput screening: a 318-target study. Sci. Rep. *14*, 7526.
70. Stahl, N., Falkman, G., Karlsson, A., Mathiason, G., and Bostrom, J. (2018). Deep convolutional neural networks for the prediction of molecular properties: challenges and opportunities connected to the data. J. Integr. Bioinform. *16*, 20180065.
71. Wallach, I., and Heifets, A. (2018). Most ligand-based classification benchmarks reward memorization rather than generalization. J. Chem. Inf. Model. *58*, 916–932.
72. Wallach, I., Dzamba, M., and Heifets, A. (2015). AtomNet: a deep convolutional neural network for bioactivity prediction in structure-based drug discovery. Preprint at arXiv. https://doi.org/10.48550/arXiv.1510.02855.
73. Leggio, L., L'Episcopo, F., Magrì, A., Ulloa-Navas, M.J., Paternò, G., Vivarelli, S., Bastos, C.A.P., Tirolo, C., Testa, N., Caniglia, S., et al. (2022). Small extracellular vesicles secreted by nigrostriatal astrocytes rescue cell death and preserve mitochondrial function in parkinson's disease. Adv. Healthc. Mater. *11*, e2201203.

STAR★METHODS

KEY RESOURCES TABLE

REAGENT or RESOURCE	SOURCE	IDENTIFIER
Antibodies		
Mouse monoclonal anti-human CD326 (EpCaM) (clone MH99), Alexa Fluor™ 488	Invitrogen	Cat#53-8326-42; RRID AB_11219279
Mouse monoclonal anti-cytokeratine 19 (clone RCK108)	Invitrogen	Cat#MA1-06329; RRID AB_559775
Mouse monoclonal anti-cytokeratine 7 (clone OV-TL12/30)	Novus Biologicals	Cat#NBP2-44814; RRID: AB_422550
Recombinant Rabbit monoclonal anti-Ki67 (clone SP6)	Invitrogen	Cat#MA5-14520; RRID AB_10979488
Goat anti-Mouse IgG (H+L) Cross-Adsorbed Secondary Antibody, Alexa Fluor™ 488	Invitrogen	Cat#A-11001; RRID AB_2534069
Goat anti-Rabbit IgG (H+L) Cross-Adsorbed Secondary Antibody, Alexa Fluor™ 647	Invitrogen	Cat#A-21244; RRID AB_2535812
Mouse-Anti-VDAC1 [N152B/23R]	Addgene	Cat# 184197-rAb; RRID: AB_2909559
Mouse-anti-β-Actin	Cell Signaling Technology	Cat# 2146; RRID: AB_2210545
HRP-conjugate Goat anti-Mouse IgG (H+L)	Invitrogen	Cat# 62-6520; RRID: AB_2533947
Bacterial and virus strains		
E.coli DH5-alpha	Invitrogen	Cat# 18265017
E.coli M15	Qiagen	N/A
Biological samples		
Patient-derived iCCA and non-tumor biopsies	Fondazione IRCCS Policlinico San Matteo, Pavia, Italy	Prot. 20200020546
Chemicals, peptides, and recombinant proteins		
Tissue storage solution	Miltenyi Biotech	Cat#130-100-008
Dulbecco's Modified Eagle's Medium (DMEM) Mixture F-12 Ham	Sigma-Aldrich	Cat#D8437
Fetal Bovine Serum (FBS)	GIBCO	Cat#10270-106
Dulbecco's Phosphate Buffered Saline (DPBS)	GIBCO	Cat#14190-094
ACK lysing buffer	GIBCO	Cat#A1049201
Cultrex UltiMatrix Reduced Growth Factor (RGF) Basement Membrane Extract (BME)	R&D Systems	Cat#BME001-10
Recovery Cell Culture Freezing Medium	GIBCO	Cat#12648010
Cultrex Organoid Harvesting Solution	R&D Systems	Cat#3700-100-01
Advanced DMEM/F-12	GIBCO	Cat#12634010
Penicillin-Streptomycin	GIBCO	Cat#15140-122
GlutaMax I	GIBCO	Cat#35050061
HEPES Buffer	GIBCO	Cat#15630056
B-27 supplement (without Vitamin A)	GIBCO	Cat#12587010
N-2 supplement	GIBCO	Cat#17502048
Nicotinamide	Sigma-Aldrich	Cat#N0636
N-acetyl-L-cysteine	Sigma-Aldrich	Cat#A9165
Forskolin	Tocris	Cat#1099/10
Y-27632 dihydrochloride (ROCK inhibitor)	Tocris	Cat#1254/1
A83-01	Sigma-Aldrich	Cat#SML0788
[Leu^{15}]-gastrin I human	Sigma-Aldrich	Cat#G9145

(*Continued on next page*)

Continued

REAGENT or RESOURCE	SOURCE	IDENTIFIER
Recombinant human epidermal growth factor (EGF) protein	R&D Systems	Cat#236-EG-200
Hepatocyte growth factor / Scatter Factor (HGF/SF)	Homemade	Gherardi et al.[64] de Nola et al.[63]
3dGRO$_{TM}$ R-Spondin-1 Conditioned Media Supplement	Sigma-Aldrich	Cat#SCM104
3dGRO$_{TM}$ L-WRN Conditioned Media Supplement	Sigma-Aldrich	Cat#SCM105
Paraformaldehyde (PFA)	Sigma-Aldrich	Cat#158127
Tween20	PanReac AppliChem	Cat#A4974
Triton X-100	Sigma-Aldrich	Cat#T8787
Bovine Serum Albumin (BSA)	Pan Biotech	Cat#P06-1391500
Hoechst33342	Invitrogen	Cat#H1399
Prolong™ Glass Antifade Mountant	Invitrogen	Cat#P36982
Trypan Blue Stain 0,4%	Logos Biosystems	Cat#T13001
Dimethyl Sulfoxide (DMSO)	Sigma-Aldrich	Cat#472301
Luria-Bertani (LB) broth	Sigma Aldrich	Cat# 1003568630
Kanamycin	Fisher BioReagents	Cat# BP906-5
Ampicillin	Fisher BioReagents	Cat# BP1760-25
Tris Base	Fisher BioReagents	Cat# BP152500
EDTA	EDM Millipor	Cat# 324503
Sucrose	Sigma Aldrich	Cat# S0389
Sodium chloride	Fisher BioReagents	Cat# S271500
$CaCl_2$	Millipore	Cat# 208291
N,N-Dimethyl-1-Dodecanamine-N-Oxide (LDAO)	Anatrace	Cat# D360
Imidazole	Sigma Aldrich	Cat# 8221840500
Dithiothreitol (DTT)	Invitrogen	Cat# D1532
Protease inhibitor cocktail	Roche	Cat# 5056489001
HisTrap HP 5 mL column	Cytiva	Cat# 17524802
Superdex 200 increase 10/300 column	Cytiva	Cat# 28990944
Amicon Ultra-30KDa	Millipore	Cat# UFC803024
Coomassie	Sigma Aldrich	Cat# 1.12553
PMSF Protease inhibitor	Thermo-Scientific	Cat# 36978
Pepstatin A protease inhibitor	Thermo-Scientific	Cat# 78436
Leupeptin Protease inhibitor	Thermo-Scientific	Cat# 78435
DNasi I	Sigma Aldrich	Cat# 11284932001
Bovine Calf Serum	Sigma Aldrich	Cat# 12133C
penicillin/streptomycin	Thermo-Fisher Scientific	Cat# 15140122
Trypsin-EDTA	Thermo-Fisher Scientific	Cat# 15400054
Isopropyl-β-D-thiogalactopyranoside (IPTG)	Sigma Aldrich	Cat# I5502
Nitrocellulose membrane (AmershamProtran 0.45 μM NC)	GE Healthcare Life Sciences	Cat# 10600002
Dulbecco's modified Eagle's medium (DMEM) - high glucose	Sigma Aldrich	Cat# D6429
McCoy's 5alpha (modified) -Medium	Thermofisher	Cat# 16600082
N,N – Dimetilfortmammide (DMF)	Sigma Aldrich	Cat# 270547
NADH – Disodium Salt	Merck	Cat# 481913
Pyruvate	Sigma Aldrich	Cat# P2256
Malate	Sigma Aldrich	Cat# M1000
Glutamate	Sigma Aldrich	Cat# G1626
Succinate	Sigma Aldrich	Cat# S2378

(*Continued on next page*)

Continued

REAGENT or RESOURCE	SOURCE	IDENTIFIER
Carbonyl cyanide 3-chlorophenylhydrazone (CCCP)	Sigma Aldrich	Cat# C2759
Rotenone	Sigma Aldrich	Cat# R8875
Antimycin A	Sigma Aldrich	Cat# A8674
Digitonin	Sigma Aldrich	Cat# D5628
Mir05	Oroboros Instrument	N/A
SnakeSkin™ Dialysis Tubing	Thermo-Fisher Scientific	Cat# 88242
BSA Bovine Serum Albumin	Sigma Aldrich	Cat# 6003
3-(4,5-dimethyl thiazolyl-2)-2,5-diphenyl tetrazolium bromide (MTT)	Sigma Aldrich	Cat# 2128
3-(1,3-benzothiazol-2-yl)-1-(3-bromophenyl)-4,4,4-trifluoro-3-hydroxybutan-1-one (VA-C1)	Enamine	Cat# Z285139336
2-[1-(2-fluorophenyl)ethylsulfanylmethyl]-3H-[1]benzofuro[3,2-ayd]pyrimidin-4-one (VA-C4)	Enamine	Cat# Z1116585429
[2-[[3-[(2-chlorophenyl)methyl]-1,3-thiazol-2-ylidene]amino]-2-oxoethyl] 5-methylthiophene-2-carboxylate (VA-C6)	Enamine	Cat# Z19760106
[2-(N-acetyl-2-fluoroanilino)-1,3-thiazol-4-yl]methyl thiophene-3-carboxylate (VA-D10)	Enamine	Cat# Z82156309
3-[(4-chlorophenyl)methylidene]thiochromen-4-one (VA-D11)	Enamine	Cat# Z46611503
Recombinant mouse VDAC1	This paper	N/A
Recombinant mouse VDAC1_N238K	This paper	N/A
Recombinant mouse VDAC1_N238R	This paper	N/A
Recombinant mouse VDAC1_N238F	This paper	N/A
Recombinant mouse VDAC1_N207R	This paper	N/A
Recombinant mouse VDAC1_N218Y	This paper	N/A
Recombinant mouse VDAC1_K236A	This paper	N/A
Recombinant mouse VDAC1_F18A	This paper	N/A
Critical commercial assays		
Tumor Dissociation Kit and gentleMACS Dissociator	Miltenyi Biotech	Cat#130-095-929
CellTiter-Glo 3D Cell Viability Assay	Promega	Cat#G9681
Total RNA Purification Plus kit	Norgen Biotek Corp	Cat#48400
Reverse Transcriptase SuperMix kit LunaScript™	New England Biolabs® Inc.	Cat#E3010L
Universal qPCR MasterMix Luna®	New England Biolabs® Inc.	Cat#M3003L
Pierce™ ECL Western Blotting Substrate	Thermo Scientific	Cat# 32106
Pierce™ Bradford Plus Protein Assay Reagent	Thermo Scientific	Cat# 23238
Deposited data		
Raw and analyzed data	This paper	N/A
Experimental models: Cell lines		
SKBR-3	ATCC	Cat # HTB-30
NIH-3T3	ATCC	Cat # CRL-1658
Oligonucleotides		
FW_qPCR_hβ-actin: ACACTGTGCCCATCTACGAG	Reina et al.[65]	N/A
Rev_qPCR_hβ-actin: AATGTCACGCATTTCCC	Reina et al.[65]	N/A
FW_qPCRhVDAC1: TCCAGCCTGATAGGTTTAG	Reina et al.[65]	N/A
Rev_qPCRhVDAC1: TTCTAAGGTAGCTATGCTGC	Reina et al.[65]	N/A

(*Continued on next page*)

Continued

REAGENT or RESOURCE	SOURCE	IDENTIFIER
Recombinant DNA		
pQE9 mouse VDAC1	Ujwal et al.[66]	N/A
pQE9 mouse VDAC1_N238K	This paper	N/A
pQE9 mouse VDAC1_N238R	This paper	N/A
pQE9 mouse VDAC1_N238F	This paper	N/A
pQE9 mouse VDAC1_N207R	This paper	N/A
pQE9 mouse VDAC1_N218Y	This paper	N/A
pQE9 mouse VDAC1_K236A	This paper	N/A
pQE9 mouse VDAC1_F18A	This paper	N/A
Software and algorithms		
Prism (GraphPad) version 8.3.0	Dotmatics	https://www.graphpad.com
ImageJ 1.53c	NIH	http://imagej.nih.gov/ij
Origin-Lab	OriginLab Corporation	https://www.originlab.com
Image-StudioLite software	Li-Cor Biosciences	https://www.licor.com/bio/image-studio/
DatLab software	Oroboros Instruments	https://www.oroboros.at
Open Babel	O'Boyle et al.[67]	N/A
AutodockVina	Eberhardt et al.[68]	N/A
Other		
Azure c600 Imaging System	Azure Biosystems	N/A
Varioskan	Thermo Scientific	N/A
Two-chamber system O2k-FluoRespirometer	Oroboros Instruments	N/A
FluoStar-Omega microplate reader	BMG LABTECH	N/A
Black opaque 96-well microplates	Costar	Cat# 3925
Prometheus Standard Capillaries	NanoTemper Technologies	Cat# PRC002
NanoTemper Tycho NT.6	NanoTemper Technologies	N/A
Bruker 700 MHz spectrometer	Bruker	N/A

RESOURCE AVAILABILITY

Lead contact

Further information and requests for resources should be directed to and will be fulfilled by the lead contact, Dr. Marco Lolicato (marco.lolicato@unipv.it).

Materials availability

Plasmids generated in this study are all derived from pQE9:mVDAC1 kindly provided by Dr. Abramson[66] and are available from the lead contact upon request.

Data and code availability

- All data reported in this paper will be shared by the lead contact upon request.
- Any additional information required to reanalyze the data reported in this paper is available from the lead contact upon request.

EXPERIMENTAL MODEL AND STUDY PARTICIPANT DETAILS

Bacterial strains

E. coli DH-5-*alpha* was used for plasmid handling. *E. coli* M15 (Kanamycin-resistant) was used for VDAC1 recombinant expression. *E. coli* strains were grown at 37°C in Luria-Bertani (LB) broth (Sigma) supplemented with the appropriate antibiotics. Antibiotics were used at the following concentrations: Kanamycin (50 μg/mL) and Ampicillin (100 μg/mL).

Cell line culture

SKBR-3 (Cat # HTB-30) and NIH-3T3 (Cat # CRL-1658), were purchased from the American Tissue Culture Collection (ATCC). SKBR-3 cells were grown in McCoy's 5A Medium supplemented with 10% fetal bovine serum (FBS), 100 units/mL penicillin and 100 μg/mL streptomycin. NIH-3T3 cells were grown in Dulbecco's Modified Eagle's Medium (DMEM) high glucose with the addition of 10% Calf Bovine Serum (CBS), 100 units/mL penicillin and 100 μg/ mL streptomycin. Both cell lines were maintained in 5% CO_2/air at 37°C. All experiments were performed when cells reached 70– 80% confluency.

METHOD DETAILS

In silico screening

Commercially available libraries of millions of chemical compounds (MCule (10M) [mcule database. https://mcule.com/database/] and Enamine in-stock (2.5M) [https://enamine.net/compound-collections/screening-collection] have been screened by Atomwise using its deep learning-based computational drug discovery platform (AtomNet™).[69–72] After rescoring and selection, 70 compounds were purchased from Enamine and tested experimentally.

Docking simulations

Docking simulations have been performed using the free software AutodockVina[68] with the mouse VDAC1 crystal structure (PDB: 3EMN) as target protein and the 3D structures of VA molecules generated with Open Babel[67] as flexible ligands.

Protein expression and purification

Mouse VDAC1 (mVDAC1) wild-type and mutant constructs were expressed as reported in.[66] Briefly, mVDAC1 and mutants cloned in pQE9 vector were transformed into M15 *E. coli* for protein expression. Cells were grown at 37°C in LB medium until OD600=0.6 and induced for 4 h with 1 mM IPTG. Cells were harvested and resuspended in lysis buffer (50 mM Tris-HCl, 2 mM EDTA, 20% sucrose, pH 8.0). The re-suspended pellet was sonicated and centrifuged (12.000 x g, 20 min) to obtain inclusion bodies. The inclusion body pellet was washed with wash buffer (20 mM Tris-HCl, 300 mM NaCl, 2 mM $CaCl_2$, pH 8.0) and solubilized in equilibration buffer (20 mM Tris-HCl, 300 mM NaCl, 6 M guanidinium hydrochloride, pH 8.0) for 3h at 4°C under stirring. Solubilized inclusion bodies were applied to the HisTrap HF 5 mL affinity column (Cytiva), washed with equilibration buffer containing 30 mM imidazole (5CV), and eluted with equilibration buffer containing 150 mM imidazole (8CV).

In vitro refolding and Size exclusion chromatography (SEC)

In vitro refolding was performed by dropwise dilution (100 μL/min) of solubilized protein into refolding buffer (25 mM Tris-HCl, 300 mM NaCl, 1 mM EDTA, 5 mM DDT, 1% (w/v) LDAO, pH 8.0) in a ratio of mg protein:ml buffer = 1:20. The procedure was carried out at 4°C for 3h. Subsequently, the refolded protein was dialyzed against dialysis buffer (25 mM Tris-HCl, 300 mM NaCl, pH 8.0) at 4°C overnight. To reduce detergent concentration, the refolded protein was applied to HisTrap HP 5ml affinity column, washed with equilibration buffer (25 mM Tris-HCl, 300 mM NaCl, 0.1% (w/v) LDAO, pH 8.0) containing 30 mM imidazole (5CV), and eluted with equilibration buffer containing 250 mM imidazole (8CV). Refolded protein was concentrated by using Amicon Ultra-30KDa and applied to a Superdex 200 increase 10/300 column (Cytiva) and eluted with SEC buffer (20 mM Tris-HCl, 50 mM NaCl, 0.1% (w/v) LDAO, pH 8.0). Protein purity and identity were verified by SDS/PAGE. Purified protein was either used immediately or flash frozen in liquid nitrogen for long-term storage. Protein stability was monitored by size-exclusion chromatography and used within 48 hours.

NMR spectroscopy

For validation by NMR spectroscopy, each compound was dissolved in d6-DMSO at a final concentration of 500 μM. ^{1}H NMR spectra were recorded at 310 K at a Bruker 700 MHz spectrometer equipped with a TXI probe, with an acquisition time of 2.36 s, inter-scan delay of 8 s, 4 dummy scans and 32 scans. The spectra were processed in Topspin by applying gaussian broadening (GB 0.02, LB -0.1 Hz) and baseline corrected. ^{19}F NMR spectra were recorded on the same samples at a Bruker 800 MHz spectrometer equipped with a TXI probe with the ^{1}H channel tuned to the ^{19}F Larmor frequency at 752.9 MHz. The spectra were recorded at 298 K with an acquisition time of 0.56 s, inter-scan delay of 5 s, 0 dummy scans and 256 scans, and processed by applying exponential broadening (LB 2 Hz). For protein-ligand interaction experiments, each compound was dissolved at a final concentration of 100 μM in 20 mM Tris HCl buffer, 50 mM NaCl, 0.1% (w/v) LDAO, pH 8.0 either in the absence or in the presence of 5 μM VDAC1 diluted from a 115 μM stock solution in the same buffer. ^{19}F NMR spectra were recorded at 298 K with an acquisition time of 0.56 s, inter-scan delay of 1 s, 0 dummy scans and 256 scans, and processed by applying exponential broadening (LB 2 Hz).

Fluorescence Polarization assay

All Fluorescence Polarization measurements were performed on a FluoStar-Omega microplate reader (BMG LABTECH) in black opaque 96-well microplates (Costar #3925) with excitation and emission wavelengths of 482 nm and 530 nm, respectively. Fluorescence polarization

assay was carried out by titrating mVDAC1 wild-type and mutants (N238K and K236A) with 5 μM NADH. The fluorescence polarization was calculated using the following equation:

$$FP = \frac{F_{parallel} - F_{perpendicular}}{F_{parallel} + F_{perpendicular}}$$

where FP is the fluorescence polarization reading, F-parallel is the fluorescence intensity parallel to the excitation plane, and F-perpendicular is the fluorescence intensity perpendicular to the excitation plane. The dissociation constant (KD) was obtained by fitting the fluorescence polarization values and the corresponding protein concentrations into a nonlinear regression model in Origin Lab. For the FP competition assays, different concentrations of VA molecules were titrated against 7 μM of VDAC1 and 5 μM of NADH. The KD was obtained by fitting the fluorescence polarization values and the corresponding VA molecules concentrations into a Hille curve. All experiments were performed in triplicates using 100 μL per well in 20 mM Tris, 50 mM NaCl, 0.1% (w/v) LDAO, pH 8.0.

Thermostability assay

For the thermal denaturation assay, mVDAC1 and mutants (at a final concentration of 0.9 mg/ml) in SEC buffer were pre-treated with 1 mM of VA molecules or 0.5 % DMF (as control) for 1h at 4°C. Subsequently, samples were loaded into quartz capillaries (Nano-Temper Technologies, Germany), and experiments were carried out using the NanoTemper Tycho NT.6 (NanoTemper Technologies, Germany). The temperature gradient was set to an increase of 30°C/min from 35°C to 95°C. Protein unfolding was measured by detecting the temperature-dependent change in tryptophan fluorescence at emission wavelengths of 330 and 350 nm. Inflection temperatures (T_i) were determined by detecting the maximum of the first derivative of the fluorescence ratios (F350/F330), using the internally automated evaluation features of the NT.6 instrument. The inflection temperatures obtained from the NanoTemper Tycho software were confirmed by averaging the fluorescence values and fitting them with the Hill equation. The variation of T_i between treated (T_{iT}) and untreated (T_{iU}) samples was calculated by the formula $\Delta T_i = T_{iU} - T_{iT}$. To quantify the effect of mVDAC1 mutations in modifying VA molecules stability, $\Delta\Delta T_i$ was calculated with the formula $\Delta\Delta T_i = \Delta Ti_{WT} - \Delta Ti_{Mut}$. Positive values of $\Delta\Delta T_i$ show the stabilizing influence of mutations, while negative values denote the destabilizing effect of mutations. All measurements were repeated at least three times.

Cell viability assays

For cell viability assay, each cell line was treated with different VA molecules concentrations for 48 h. Subsequently, the cells were used for cell viability assay. Cell viability was evaluated by 3-(4,5-dimethyl thiazolyl-2)-2,5-diphenyl tetrazolium bromide (MTT) assay. SKBR-3 and NIH-3T3 cell lines were plated in 96-well plates at 10.000 cells/well and after 24 h received the indicated treatment. Subsequently, MMT was added to the culture medium to reach a final concentration of 5 mg/ml. After incubation at 37°C for 3 h, the medium was removed, and the formazan crystals produced were dissolved by adding 100 μl of dimethyl sulfoxide. The absorbance at 590 nm was determined using the microplates reader Varioskan (Thermo Scientific).

High-resolution respirometry

The characterization of mitochondrial respiration in the SKBR-3 and NIH-3T3 cell lines was performed by High-Resolution Respirometry using the two-chamber system O2k-FluoRespirometer (Oroboros Instruments, Innsbruck, Austria). The whole respiratory profiles of SKBR-3 and NIH 3T3 cell lines, exposed or not to 10μM of small molecules for 48 h, were determined by a specific substrate-uncoupler-inhibitor titration (SUIT) protocol as in[73] in mitochondrial respiration buffer Mir05 (Oroboros Instruments) at 37°C under constant stirring of 750 rpm. Plasma membranes of intact cells were mildly permeabilized with 3μM digitonin and the non-phosphorylating respiration (LEAK) was measured in the absence of adenylates. Oxygen flow-related N-pathway was attained by the addition of pyruvate (5 mM), glutamate (10 mM), malate (2 mM), and ADP (2.5 mM). NS-pathway was then activated by supplementation with 10 mM succinate. The maximal capacity of electron transport (ET) chain was determined by titration with the uncoupler carbonyl cyanide 3-chlorophenylhydrazone (CCCP, 0.5 μM) up to the complete dissipation of the proton gradient. Finally, the residual oxygen consumption (ROX) was achieved by inhibiting the ET chain with 2 μM rotenone and 2.5 μM antimycin. Oxygen fluxes corresponding to LEAK, N-, NS-pathway and ET maximal capacity were normalized for the ROX and expressed as pmol/s per million cells (Table S3). The oxygen flows linked to ATP production were calculated as the difference between the NS-pathway and the LEAK respiration.[48] Respiratory states of cells exposed to VA molecules were normalized to their respective untreated controls and shown as mean ± SEM of n=3 in three independent experiments. Data were statistically analyzed by unpaired t-test using Prism software (GraphPad, San Diego, CA, co USA). The following values * $p < 0.05$, ** $p < 0.01$, *** $p < 0.001$ were taken as significant. Instrumental and chemical background fluxes were calibrated as a function of the oxygen concentration using DatLab software (Oroboros Instruments).

Western blots

1 x 10^6 cells for each line were collected and lysed in extraction buffer (50 mM Tris, 150 mM NaCl, EDTA 1 mM, 1% TRITON X-100, pH 7.4, and protease inhibitors). After lysis, the supernatant was collected, and the protein content was estimated with the Bradford reagent with bovine serum albumin (BSA) as a standard. 50 μg of total protein of each sample were separated using SDS/PAGE electrophoresis, transferred to a nitrocellulose membrane (AmershamProtran 0.45 μM NC; GE Healthcare Life Sciences), and blocked in 5 % (w/v) BSA at room temperature for

1h. The membranes were incubated overnight at 4°C with primary antibodies against VDAC1 and β-Actin (1:5000, #2146; Cell Signaling Technology) after the washing step with secondary antibodies HRP-conjugate Goat anti-Mouse IgG (H+L) (1:5000, #89842, Invitrogen), HRP-conjugate Goat anti-Rabbit IgG (H+L) (1:5000, #31460, Invitrogen). Chemiluminescent detection was performed using Pierce™ ECL Western Blotting Substrate. The membranes were read using the Azure c600 Imaging System (Azure Biosystems). For the western-blot analysis, data were analyzed with Image-StudioLite software (Li-Cor Biosciences), and β-Actin was used as an internal loading control. Data were statistically analyzed by one-way ANOVA followed by Dunnett's multiple comparisons test.

Primary cells cultivation and organoid generation

For organoid generation, surgically resected iCCA specimens along with matched non-tumoral tissue from a non-adjacent liver site were obtained from treatment-naïve patients at Fondazione IRCCS Policlinico San Matteo, Pavia, Italy. Tissue samples were stored in tissue storage solution (Miltenyi Biotec, Bergisch Gladbach, Germany) and processed within 24 hours. A written informed consent was obtained from each individual. The study protocol is compliant with the ethical guidelines of the 1975 Declaration of Helsinki and was approved by our institutional ethical committee. Briefly, tissue samples were treated by enzymatic and mechanical dissociation with the human Tumor Dissociation Kit and gentleMACS Dissociator, according to the manufacturer's instructions (Miltenyi Biotec). The cell suspension was filtered in a 70 μm cell strainer and centrifuged twice at 50 xg for 2 min. The cell pellet was then incubated in 1ml of ACK lysing buffer (GIBCO) to remove blood cells. After cell counting, about 15.000 cells per well were resuspended in Cultrex UltiMatrix Reduced Growth Factor (RGF) Basement Membrane Extract (BME) (R&D Systems) and seeded in pre-heated low adhesion 24-well plates (GreinerBio). The remaining cells were cultured in Dulbecco's Modified Eagle's Medium (DMEM)/F-12 (Sigma-Aldrich) with 10% Fetal Bovine Serum (FBS) (GIBCO), and 1% penicillin/streptomycin (GIBCO) and seeded in T25 flask, in order to generate bidimensional primary cell lines. After BME droplets polymerization at 37°C, an expansion medium was added. The expansion medium was adapted from the protocol of Nuciforo et al. (2018)[42] and composed of Advanced DMEM/F-12 (GIBCO) with 1% penicillin/streptomycin (GIBCO), 1% Glutamax (GIBCO), 10 mM HEPES (GIBCO) with the addition of B-27 (1:50) (GIBCO), N-2 (1:100) (GIBCO), 10 mM nicotinamide (Sigma-Aldrich), 1.25 mM N-acetyl-L-cysteine (Sigma-Aldrich), 10 μM forskolin (Tocris), 10 μM Y-27632 dihydrochloride (ROCK inhibitor) (Tocris), 5 μM A83-01 (Sigma-Aldrich), 10 nM [Leu15]-gastrin I (Sigma-Aldrich), 50 ng/ml epidermal growth factor (EGF) (R&D Systems), 25 ng/ml hepatocyte growth factor/scatter factor (HGF/SF) (Homemade), 10% R-Spondin1 conditioned medium (Sigma-Aldrich) and 30% Wnt3a conditioned medium with Noggin (Sigma-Aldrich). The passage of the organoids was performed periodically in a 1:2-1:5 split ratio, every 7-10 days, by incubation in Cultrex Organoid Harvesting Solution (R&D Systems) for 1 hour on ice and mechanical dissociation with a pipette. For freezing, the organoids were dissociated and resuspended in Recovery Cell Culture Freezing Medium (GIBCO) and then cryopreserved.

Drug treatment

Tumor and non-tumor organoids were plated in 20 μl of BME droplets in 48-well plates in order to develop organoids. After 3 days, VA small molecules (D10, C1, and C4) at different concentrations were resuspended in expansion medium with the addition of 0.02% of Tween20, and cell viability was measured after 72 hours, using CellTiter-Glo 3D Cell Viability Assay (Promega). Also, tumor and paired-non tumor bidimensional cell lines were seeded at density of 5.000 cells per well in 96-well plates, and after 3 days treated with VA small molecules at different concentrations, and viability was evaluated by MTT assay after 72 hours. Luminescence and absorbance respectively were measured on Polarstar-Omega microplate reader (BMG LABTECH). Results were normalized to vehicle (100% DMSO).

RNA extraction and quantitative real time PCR (RTPCR)

Total RNA was extracted from tumor and paired non-tumor primary cell cultures using Total RNA Purification Plus kit (Norgen Biotek Corp) in accordance with the manufacturer's instructions. cDNA was synthesized using 400 ng of total RNA and a Reverse Transcriptase SuperMix kit LunaScriptTM (New England Biolabs® Inc.). cDNA was amplified with Universal qPCR MasterMix Luna® (New England Biolabs® Inc.) and using gene-specific primers. All targets were amplified on a CFX96 Connect Real-Time PCR Detection System (Biorad). Expression levels were normalized to the expression of the housekeeping gene β-ACTIN.

Immunofluorescence staining

In order to perform an immunofluorescence characterization, organoids were fixed in cold 4% paraformaldehyde (Sigma-Aldrich) for 40 minutes at 4°C and subsequently resuspended in PBS with 0.1% Tween20 (PanReac Applichem) for 10 minutes at 4°C for the permeabilization phase. To reduce background non-specific staining, organoids were blocked in PBS with 0.1% Triton X-100 (Sigma-Aldrich) and 2% Bovine Serum Albumin (Pan Biotech) solution, for 1h at room temperature, and then incubated with primary antibodies Epithelial Cell Adhesion Molecule (EpCaM, 1:250; Invitrogen), cytokeratine 19 (CK19, 1:250; Invitrogen), cytokeratine 7 (CK7, 1:250; Novus Biologicals), and Ki67 (1:250; Invitrogen) overnight at 4°C. Fluorochrome-labeled secondary antibodies (1:500; Invitrogen) in PBS solution with 0.1% Triton X-100 and 0.5% BSA were incubated for 1h at room temperature. Nuclei were counterstained with Hoechst33342 (Invitrogen). Confocal images were captured on a Leica SP5 inverted confocal microscope (Leica). Images were processed using ImageJ software.

QUANTIFICATION AND STATISTICAL ANALYSIS

Statistical analysis

For statistical analysis, GraphPad Prism was used. Curve fitting in cell viability was performed using Prism (GraphPad) software and the nonlinear regression equation. All experiments were performed at least three independent times and results are shown as mean ± SEM. Immunofluorescence imaging results were analyzed based on z stacks acquired with confocal microscope. Significance is opportunely stated in main text or figure legends.